Journal of Volcanology and Geothermal Research 364 (2018) 20–34

Contents lists available at ScienceDirect

Journal of Volcanology and Geothermal Research

journal homepage: www.elsevier.com/locate/jvolgeores

Origin of late Miocene Peraluminous Mn-rich Garnet-bearing Rhyolitic Ashes in the Andean Foreland (Northern Argentina)

Beatriz Coira [a,*], Suzanne Mahlburg Kay [b], José G. Viramonte [c], Robert W. Kay [b], Claudia Galli [a,d]

[a] INECOA-CONICET, Instituto de Geología y Minería, Av. Bolivia 1661, 4600 S.S. de Jujuy, Argentina
[b] Dept. Earth and Atmospheric Sciences, Snee Hall, Cornell University, Ithaca, NY 14853, USA
[c] Instituto Geonorte, Universidad Nacional de Salta, INECO UNSa-CONICET, Av. Bolivia 5150, 440 Salta, Argentina
[d] Facultad de Ciencias Naturales, Universidad Nacional de Salta, Av., Bolivia 5150, 4400 Salta, Argentina

ARTICLE INFO

Article history:
Received 9 May 2018
Received in revised form 9 August 2018
Accepted 25 August 2018
Available online 7 September 2018

Keywords:
Magmatic spessartine-rich garnet
Central Andean Puna plateau
Plinian rhyolite eruption
Andean foreland garnet-bearing tuffs
Ramadas Volcanic Center

ABSTRACT

The Ramadas Volcanic Center on the eastern margin of the central Andean Puna plateau along the Olacapato-El Toro lineament in Argentina erupted a rare strongly peraluminous Mn-rich garnet-bearing rhyolitic tuff in the late Miocene. The voluminous ashes from this eruption, which are distinctive in having euhedral spessartine almandine garnets ($Alm_{70–72}Sps_{22–26}Grs_{2–4}Prp_{0.5–1}$) as their only phenocryst, are widely dispersed in the Andean foreland. Among these tuffs are those in the Guanaco Formation foreland basin sediments along the Xibi-Xibi and Los Alisos rivers in the Rio Grande de Jujuy basin and the Metán Valley, some 100–200 km east of the Ramada Volcanic Center. The co-occurrence of tubular to cellular pumice fragments and blocky glass shards in an ash matrix in these tuffs is interpreted as indicating that they erupted in an initial vent-opening event with pulsating pyroclastic surges at the initiation of the strong Plinian eruption of the Ramada Volcanic Center. New Ar/Ar ages from the Guanaco Fm. glass shards agree with fossil ages in placing the eruption at ~6.3 ± 0.3 Ma. A number of distinctive chemical, isotopic and mineralogical features including Mg-rich biotite and Mg-hastingsite xenocrysts of the Guanaco Formation and Ramadas Volcanic Center tuffs are consistent with the melt having been derived by extensive crystallization of a mantle-derived mafic shoshonitic series magma contaminated by assimilation/dehydration melts of metapelitic sediment and the Puna crust. Distinctive chemical features include whole rock SiO_2 contents of ~75–76% wt%; A/CNK indices >1.2; low Ca, Mg, Ti, and Fe concentrations; steep REE patterns with extreme negative Eu anomalies; low Ba, Sr, LREE and high Cs, Rb, U concentrations; and recalculated initial ratios of $^{87}Sr/^{86}Sr$ at ~0.7119 and $^{143}Nd/^{144}Nd$ of ~0.5123 at 6.3 Ma. The erupted magma has a transitional chemical character between those of the ~11 Ma Mn-rich garnet-bearing Coyaguayma ignimbrites to the north and the ~6 Ma Cerro Galan ignimbrites to the south. Unlike these crystal-rich ignimbrites, the Ramadas tuff records the extraction of an extensively fractioned melt from a plagioclase, K-feldspar, quartz and biotite-bearing mush with accessory titanomagnetite and apatite. In line with existing experimental studies on Mn-rich garnets and comparisons with the Coyaguayma ignimbrite, pre-eruption crystallization of the rhyolite segregated from the mush likely occurred at ~800° to 720 °C at a depth of no <15–12 km as the H_2O content increased from ~4–5% to ~7.5%. Mn-rich garnet was the only phase to be crystallized in the melt extracted from the mush before the eruption, whose rapid rise was facilitated by extension along the Olacapato-El Toro lineament.

1. Introduction

Spessartine-almandine garnet-bearing silicic rhyolites and tuffs are uncommon in the geologic record and very rare in the central Andes. However, they occasionally occur in the widespread volcanic ash beds in the Neogene deposits of the Andean foreland basin in northwestern Argentina and in a few rare silicic volcanic localities like the Ramadas Volcanic Center (e.g. Viramonte et al., 1984), the Coyaguayma Ignimbrite (Caffe et al., 2012) and the Botijuela deposits (Richards et al., 2006) in the Puna (Fig. 1). Here, we use the garnet-bearing tuffs in the Guanaco Formation in the Río Grande de Jujuy and Metán valleys of the Cordillera Oriental (Figs.1 and 2) to correlate and constrain the age of the foreland basin deposit, tie these tuffs to the Corte Blanco tuffs that erupted from the Ramadas Volcanic Center some 100–200 km to the west and discuss the origin of these silicic tuffs whose garnet phenocrysts are among the most spessartine-rich in igneous rocks.

We present new petrographic and mineral analyses, whole rock major and trace element, analyses and Ar/Ar glass ages for the distal garnet-bearing pyroclastic air fall deposits in the Guanaco Formation

* Corresponding author.
E-mail address: bcoira2015@gmail.com (B. Coira).

https://doi.org/10.1016/j.jvolgeores.2018.08.020
0377-0273/

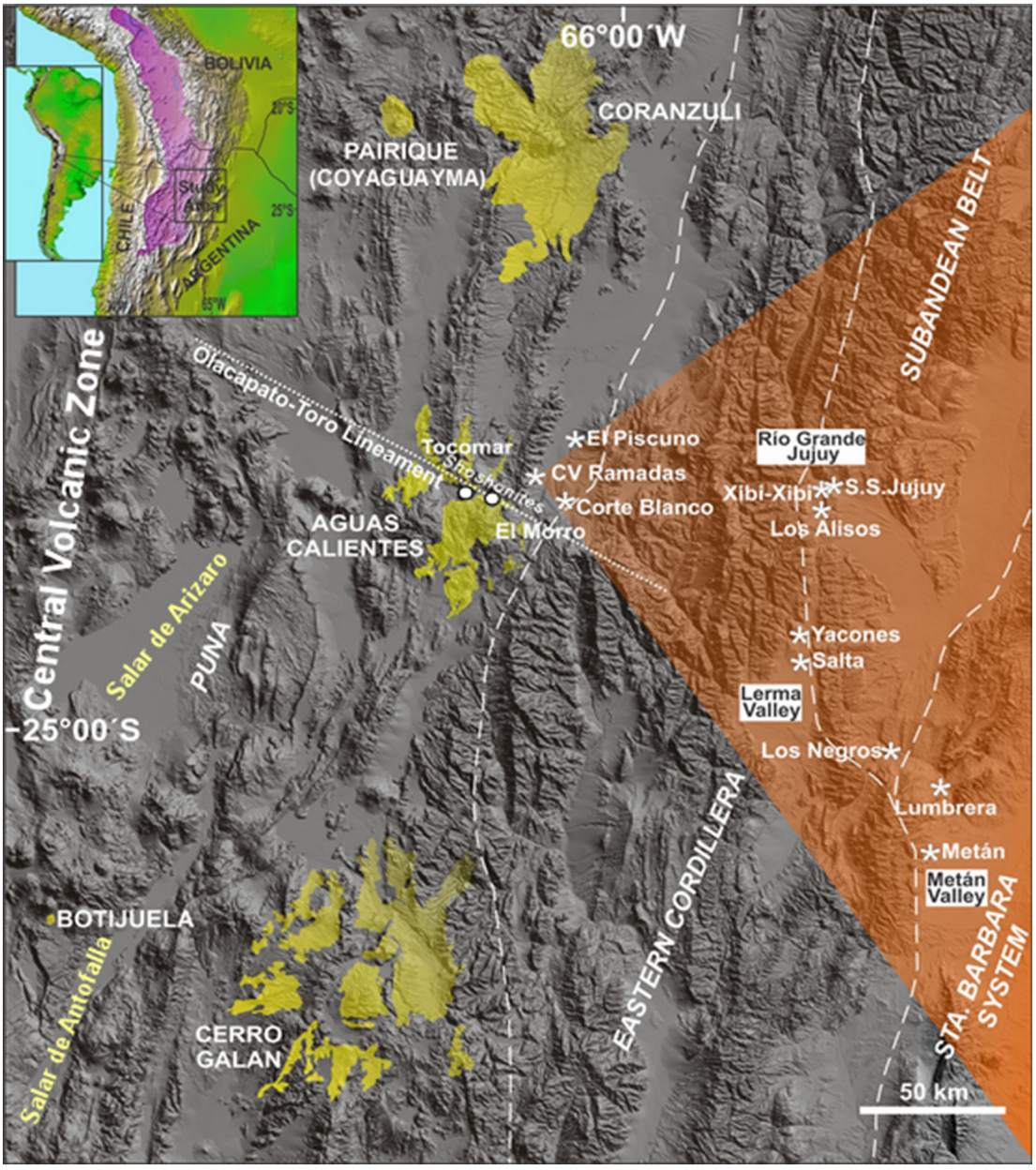

Fig. 1. Digital elevation map of the central Puna and Eastern Cordillera in Argentina showing the location of the Ramadas Volcanic Center (CV Ramadas) and general distribution of the erupted tuffs (in orange) relative to the Pairique volcanic complex, the Coranzuli ignimbrite center, the Aguas Calientes caldera complex, the El Morro volcanics, the Cerro Galán ignimbrite complex and the Botijuela volcanic center (all in yellow) and the San Geronimo and Chorrillos shoshonitic centers along the Olacapato-El Toro lineament (white circles). Asterisks mark the volcanic ash localities in the Ramadas region and the Rio Grande de Jujuy and Juramento-Metán Valleys discussed in this study. Square in inset shows the location of the region relative to South America and the region of the Central Andean Puna-Altiplano plateau.

and compare these data with new major and trace element analyses and published Sr and Nd isotopic and mineralogical data from the Corte Blanco tuffs erupted from the Ramadas Volcanic Center. These geochemical and mineralogical data provide new insights into the origin of the Ramadas Volcanic Center garnet-bearing tuffs and their differences with other spessartine-almandine garnet-bearing silicic volcanic rocks erupted in the Puna.

2. Corte Blanco Tuff, Ramadas Volcanic Center and Guanaco Fm. Garnet-bearing Tephras

2.1. The Corte Blanco Tuff and the Ramadas Volcanic Center

The Corte Blanco Tuff (Viramonte et al., 1984) is a collective name for a complex suite of peraluminous, garnetiferous rhyolitic domes and pyroclastic flows that constitute the main explosive magmatic facies from the Ramadas Volcanic Center along the Olacapato-El Toro lineament on the eastern edge of the Puna plateau (see Fig. 1). The eruption dynamics and dispersal mechanisms of these volcanic rocks, which constitute the largest plinian fall deposit on the Puna-Altiplano plateau not associated with a larger caldera complex, have been studied by Viramonte et al. (1994, 2007), Del Papa et al. (1993), Tait (2004) and Tait et al. (2009). These studies show that the distribution of the fall deposits from the plinian phase have an eastward asymmetry with the medial facies occurring ~20 km east of the vent and the distal facies reaching into the sub-Andean Belt and Santa Barbara system (Fig. 1). Fine-grained, garnet-bearing ash deposits from this eruption have been identified up to 400 km east of the vent. In a detailed study, Tait (2004) showed that the medial and distal phases are dominated by thick, plinian pumice fall deposits with subordinate intercalated

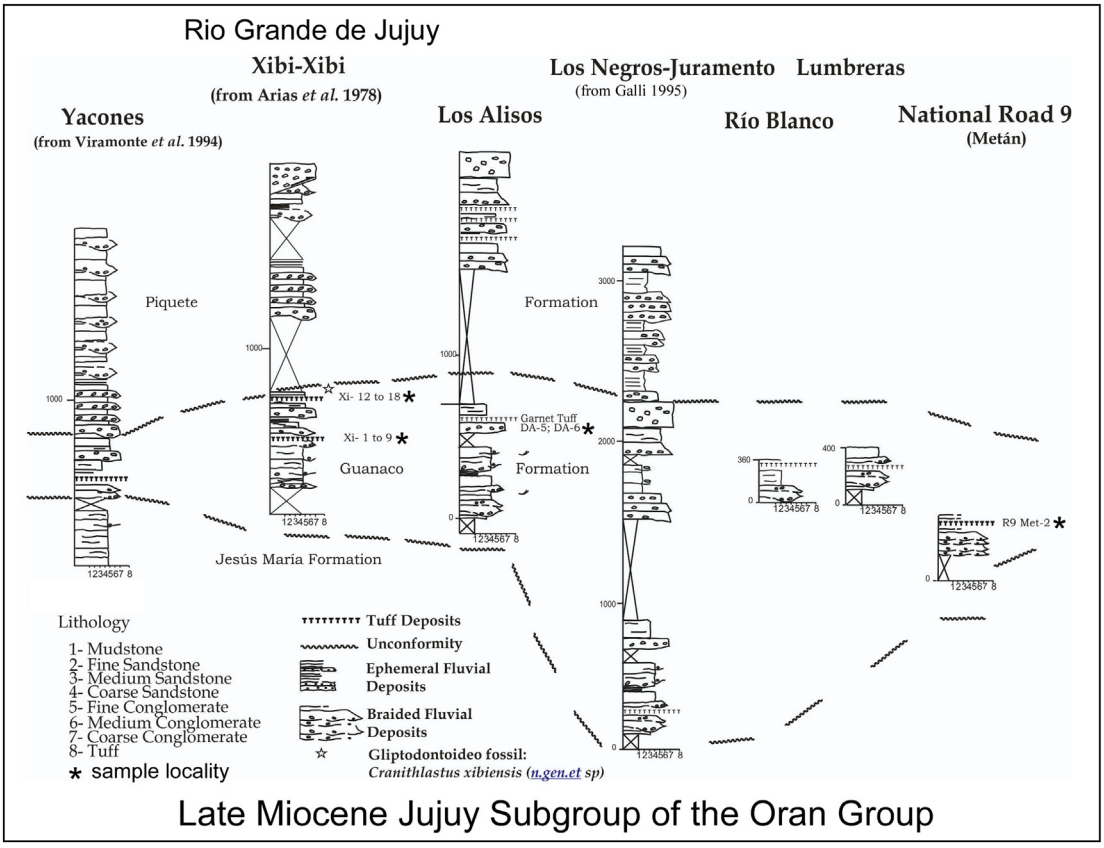

Fig. 2. Stratigraphic columns of the Miocene Jesus Maria, Guanaco and Piquete Formations in the Jujuy subgroup of the Oran Group in the Subandean Belt and Santa Barbara system showing the distribution of volcanic tuffs. The location of samples analyzed in this study are indicated by the dark stars and the Gliptodontoideo fossil locality by the open star. See text for further details and discussion.

pyroclastic surge and ignimbrite deposits. Tait (2004) and Tait et al. (2009) calculated that the ejected juvenile material had a volume in excess of 35 km^3 DRE (dense rock equivalent) and erupted from a column that rose to a height no >35 km above the vent.

2.2. Garnet-bearing Tephra in the Guanaco Formation of the Andean Foreland in Argentina

The well-exposed tephra layers in the Cenozoic strata of the Rio Grande of Jujuy and Metán valleys (Fig. 1) serve both as time-stratigraphic markers for correlating basin deposits in the foreland and as recorders of volcanic activity that put these foreland sequences into the context of the explosive silicic volcanic record to the west (Del Papa et al., 1993; Viramonte et al., 1994, 2007). Among the most valuable markers are ashes from plinian eruptions (e.g., Sparks and Walker, 1977; Chesner et al., 1991) like those from the Ramadas Volcanic Center whose co-ignimbrite ash columns can be associated with specific pyroclastic flows and eruption centers.

The Late Miocene garnet-bearing tuffs in the Rio Grande de Jujuy and Metán Valleys studied here occur in the foreland basin deposits of the Neogene Oran Group, which uncomfortably overlies the Cretaceous-Paleogene deposits of the Salta Rift basin (Salfity and Marquillas, 1994). Measured sections of Oran Group sediments from the Jesus Maria Formation in the upper part of the basal Metán Subgroup through the Guanaco and Piquete Formations in the upper Jujuy Subgroup are shown in Fig. 2. These sections are largely in the upper Jujuy subgroup, which consists of a coarsening upwards succession of sandstones to conglomerates (Gebhard et al., 1974; Russo and Serraiotto, 1978; Galli, 1995). The pyroclastic strata analyzed here are come from the Guanaco Formation in the lower Jujuy Subgroup, which is largely comprised of well-sorted sandstones and matrix-supported conglomerates with sharp transitions to mudstones (González Villa, 2002). The airfall deposits shown in the Route 9 section near Metán (Figs. 1 and 2) include the garnet-bearing tuffs that Viramonte et al. (1984, 1994) and Del Papa et al. (1993) were the first to correlate with the Corte Blanco Tuff from the Ramadas Volcanic Center.

The garnet-bearing foreland tuffs analyzed here are principally from the Guanaco Formation along the Xibi-Xibi and Los Alisos tributary rivers in the Rio Grande de Jujuy basin and in the Metán valley (Figs.1 and 2). These 2.6 to 5 m thick ash beds, which are interspersed within clastic sediments, are whitish to whitish-gray fine vitric tuffs. Some of the pyroclastic units are primary air fall tuffs as they are relatively well sorted homogeneous layers with normal or inverse grading that lack distinct internal laminae. These primary airfall beds are associated with other layers that exhibit the "resedimentation-syneruptive" characteristics of McPhie et al. (1993) including compositional uniformity or systematic changes that indicate rapid deposition (mass-flow, hyper-concentrated flow and traction currents), domains of unmodified juvenile clasts, scarce or absent lithic fragments and homogeneous sets of phenocrysts. Only ash bed layers showing primary or "resedimentation-syneruptive" characteristics were sampled in this study.

As shown in Fig. 2, the first set of Guanaco Formation samples comes from the ~1950 m thick Xibi-Xibi section with samples Xi-1 to Xi-10 coming from pyroclastic airfall deposits in the lower part of the section at 24°11′45″S, 65°19′5.9″W, and samples Xi-12 to Xi-18 coming from the upper part of the section at 24°11′28″S, 65°19′07.4″W. The sedimentary deposits hosting these ash layers largely consist of matrix-supported conglomerates with cut and fill geometries and planar cross stratification, and conglomeratic sandstones. In detail, samples Xi-1 to Xi-10 come from a five meter thick layer of primary and resedimented tuffs that overlies cross-bedded light brown sandstones and siltstones. The basal 2.2 m is a 1.3 m thick massive white fine-grained primary

tuff (sample Xi-9) that is overlain by a 0.2–0.3 m thick primary laminated tuff (sample Xi-8) and a 0.6 m resedimented cross-stratified tuff (sample Xi-7). The upper 2.8 m of the layer is composed of a sequence of 0.5–0.8 m thick layers of fine massive tuffs (samples Xi-1, Xi-3, Xi-4) interbedded with thin (5–10 cm) lapilli-tuffs (samples Xi-2 and Xi5). The only macroscopically visible minerals in these tuffs are garnet phenocrysts up to 2 mm across.

Samples Xi-12 to Xi-18 come from a 2.6 m thick ash deposit in the upper part of the section that is essentially composed of fine white tuffs interpreted as plinian fall deposits. This ash deposit begins with a 0.9 m thick massive tuff (sample Xi-17) that is overlain by a partially eroded 0.05–0.1 m thick fine tuff (sample Xi-14) and a 0.3 m thick fine homogeneous tuff (sample Xi-12). These layers are then overlain by a 0.9 m thick sequence of resedimented tuffs (not analyzed) with planar and wavy bedding. The uppermost part of this ash deposit is composed of a very thin (~5 cm) lapilli-tuff bed (not analyzed) that is overlain by a 0.4 m thick layer of a fine white normally graded tuff (sample Xi-18). As in the underlying tuff layers, the only visible minerals are garnet phenocrysts with diameters up to 2 mm. A gliptodontoideo fossil (star in Fig. 2), identified as Cranithlastusxibiensis (n.gen.et sp) and assigned to the late Miocene Huayquerian "stage" lies 195 m above this ash deposit (Arias et al., 1978).

The second set of tuff samples is from the >1630 m thick Los Alisos section exposed on Provincial Road 8 at 24°15′44.7″S, 65ª19′31″W (see Fig. 1). In this section, the basal contact with the Metán Subgroup is covered, and the Jujuy Subgroup forms part of an anticlinal structure with the Guanaco Formation in the core. Here, the Guanaco Formation consists of medium-sized matrix-supported conglomerates with cut and fill geometries and planar cross stratification along with well-sorted conglomeratic sandstones. A 1.5 m thick ash deposit intercalated between the conglomerates and the well-sorted fine sandstones contains a 0.9 m thick massive white tuff bed with pumice fragments and garnet crystals up to 1–2 mm across (sample Da-5). Along strike, this unit grades into a 0.6 m thick grayish brown tuff containing 15–20% pumice and scarce garnet crystals up to 2 mm across (sample Da-6).

The third set of samples comes from the section exposed in the Metán valley along Argentine National highway 9 at 25°25′49″S, and 64°57′16.43″W (see Fig. 1). In this locality, the Guanaco Formation is composed of gray matrix-supported conglomerates that includes a conspicuous 2.8 m thick layer of mixed primary and resedimented white ash deposits. The basal ~90 cm of this deposit consists of a very fine-grained white tuff with garnet phenocrysts up to 2 mm across (sample R9Met-2). This part of the deposit is essentially homogeneous except for a slight reverse grading in the basal 10 cm and some coarse pumice clasts that are immersed in an ash matrix in the middle of the layer. Overlying this bed is an approximately two meter thick planar to cross-bedded layer of resedimented pumice and fine ash. The upper part of this layer, which is interpreted as a plinian fall deposit, consists of an up to 10 cm thick bed of fine-grained tuff intercalated with a pumice-rich tuff.

3. Analyses of Guanaco Formation Tephra and Ramadas Volcanic Center samples

The Guanaco Formation tephra samples selected for textural and chemical analyses and dating here are all representative unaltered homogeneous pyroclastic layers with sparse or no lithic fragments. All are rich in fresh glass shards and pumice fragments and have sparse garnet grains as their only major phenocryst. The new chemical analyses of these Guanaco Formation volcanic fragments and minerals in Tables 1 to 3 are discussed below in light of new major and trace element analyses of representative obsidian, pumice and perlite samples from the Ramadas Volcanic Center in Table 4 and published mineral and whole rock analyses (Viramonte et al., 1984, 1994, 2007; Del Papa et al., 1993; Gauthier et al., 1994; Tait, 2004; Kay et al., 2010; Bardelli et al., 2017).

The major element analyses of the garnets and other minerals in the Guanaco Formation tephra (Tables 1 and 2) and the whole rock pumice and shard compositions (Table 3) were analyzed on a JEOL JXA 8230 electron microprobe in the Laboratory of Electronic Microscopy and Analysis (LAMARX) at the Universidad Nacional de Cordoba-CONICET (Argentina). The analyses were acquired at a voltage of 15 kV and a current of 20 mA using a defocused 10–20 μm beam and 10 s counting times. Concentrations were calculated relative to standards from the United States Geological Survey (USGS) with matrix corrections determined using a CIT-ZAF program.

The whole rock major and trace element compositions of the Guanaco Formation bulk tephra layers and the Ramadas Volcanic Center obsidian, pumice and perlite samples (Table 4) were analyzed using a combination of XRF analyses performed at the University of Jujuy and Instrumental Neutron Activation analyses (INAA) done at Cornell University. The analytical techniques are discussed in Kay et al. (2010). As all analyses were done directly on rock powders, there are no issues of incomplete sample dissolution as can be a problem with siliceous samples.

3.1. Mineral and glass fragments in the Guanaco Formation tephras

Petrographic studies show that the Guanaco Formation tephra samples are characterized by bubble wall shards, pumice fragments with fibrous or cellular structure and equant blocky glass shards with very low vesicularity. Their general features are similar to those of the tephra samples described by Viramonte et al. (1994) in proximal localities. As shown in photomicrographs from representative sample Xi-9 in Fig. 3a, most of the tephras show a striking contrast in the vesicularity of their juvenile clasts with both tubular to cellular pumice fragments and blocky glass shards being present. The blocky glass shards make up 30% or more of the volume with other fragments making up the rest. The individual fragments are typically 0.4–0.8 mm in diameter, generally free of microlites and set in a fine (<0.06 mm in diameter) mostly vitric (90–95%) matrix (see Fig. 3a). Less frequent lapilli tuffs are composed of >85% pumiceous, angular to sub-angular lapillus fragments (2.3–0.5 mm in diameter) set in a fine ash matrix.

Phenocrysts are scarce in the Guanaco Formation ash and lapilli beds where they make up only ~1–3% of the volume. The dominant phenocryst is garnet (Fig. 3a and b, analyses in Table 1) with the only other phenocrysts being scarce, small euhedral $Or_{97}Ab_3$ sanidine microlites (analyses in Table 2) enclosed in the glass shards. Occasional quartz grains with slight reaction borders occur within the pumice and shard fragments. Other minerals present are accessory magnetite, small monazite grains that are occasionally included in garnet, and small brownish biotite and greenish amphibole grains interpreted as xenocrysts (analyses in Table 2).

The presence of a small number of 100–400 μm garnet phenocrysts is a distinctive hallmark of the Guanaco Formation tuffs. As shown in Fig. 3a and b, the garnets occur scattered within and among the glassy shards with most being euhedral in shape. The microprobe analyses in Table 2 show them all to be Fe and Mn-rich almandine-spessartine garnets with compositions near $Alm_{70-72}Sp_{23-26}Gro_{2-4}Prp_{0.5-1}$. Nearly all are homogeneous with only a minor amount of core to rim variation in a few grains (e.g., sample DA-5 in Table 2). As shown in Table 1 and Fig. 4, the compositions of these garnets are similar to those in the tuffs at Metán, Yacones and Los Negros and in the Ramadas Volcanic Center obsidian, perlite and pumice samples analyzed by Gauthier et al. (1994) and Viramonte et al. (1994).

These garnet compositions are particularly notable for having ~10–11% wt% MnO, which equates to a spessartine content of 22–25.5% (Table 1, Fig. 4). Spessartine contents like these are in the upper range of those in a global compilation of garnet compositions in volcanic rocks and granites from Harangi et al. (2001) when plotted

Table 1
Major element composition of garnets of Guanaco Formation tuffs and Ramadas pumice and lavas.

	Xibi -Xibi						Los Alisos					Metán[a]	Yacones[a]	Los Negros[a]	Ramadas - La Pava[a]			Coyaguayma
Sample	Xi 1	Xi 1	Xi 9	Xi 9	Xi 9	Xi 13	DA5 center	DA5 interior	DA5 border	DA5 center	DA5 border				Pumice	Obsidian	Rhyolite	PQ01-40p
Oxide wt%																		
SiO_2	36.43	35.91	36.12	36.09	36.39	36.11	36.56	36.29	36.42	36.81	36.56	37.12	37.34	36.08	36.19	36.34	36.58	36.85
TiO_2	0.02	0.00	0.07	0.00	0.00	0.00	0.01	0.01	0.00	0.01	0.00	0.07	0.07	0.14	0.03	0.01	0.03	0.04
Al_2O_3	20.07	20.08	20.96	20.68	21.09	20.57	20.79	20.80	21.07	20.92	21.07	20.32	21.35	22.54	19.95	20.09	20.28	20.76
Fe_2O_3	0.48	0.37	0.00	0.00	0.00	0.00	0.00	0.00	0.00	0.00	0.00	0.00	0.00	0.00	0.69	0.28	0.18	0.15
FeO	30.50	30.27	30.62	30.00	30.86	29.14	30.14	30.34	30.32	30.97	30.32	29.80	29.12	29.94	31.48	31.45	31.45	36.82
MnO	11.11	10.81	10.35	9.70	10.22	10.08	10.25	10.26	10.19	9.90	10.19	9.56	9.20	9.13	8.99	9.80	9.97	4.25
MgO	0.14	0.15	0.18	0.19	0.12	0.14	0.17	0.17	0.25	0.21	0.25	0.27	0.24	0.13	0.28	0.16	0.18	1.13
CaO	1.17	1.27	1.22	1.26	1.20	1.17	1.10	1.16	1.24	1.18	1.24	1.23	1.29	1.01	1.88	1.22	1.24	0.8
Total	99.92	98.86	99.52	97.92	99.88	97.21	99.02	99.03	99.49	100.00	99.63	98.37	98.61	98.97	99.49	99.35	99.91	100.81
Cations based on 12 oxygens																		
Si	3.010	2.995	2.984	3.026	2.996	3.050	3.034	3.013	3.006	3.025	3.013	3.098	3.097	2.982	2.997	3.016	3.018	3.00
Aliv	0.00	0.00	0.02	0.00	0.02	0.00	0.00	0.00	0.01	0.00	0.01	0.00	0.00	0.08	0.00	0.00	0.00	0.00
Al vi	1.96	1.97	2.02	2.04	2.03	2.04	2.03	2.03	2.03	2.02	2.03	1.98	2.06	2.10	1.95	1.97	1.97	1.99
Ti	0.00	0.00	0.00	0.00	0.00	0.00	0.00	0.00	0.00	0.00	0.00	0.00	0.00	0.01	0.00	0.00	0.00	0.00
Fe^{3+}	0.03	0.02	0.00	0.00	0.00	0.00	0.00	0.00	0.00	0.00	0.00	0.00	0.00	0.00	0.04	0.02	0.01	0.01
Fe^{2+}	2.11	2.11	2.14	2.14	2.15	2.10	2.12	2.13	2.12	2.15	2.12	2.11	2.10	2.18	2.18	2.18	2.17	2.50
Mn	0.78	0.76	0.72	0.68	0.71	0.71	0.71	0.72	0.71	0.68	0.71	0.67	0.63	0.63	0.63	0.69	0.70	0.29
Mg	0.02	0.02	0.02	0.02	0.01	0.02	0.02	0.02	0.03	0.03	0.03	0.03	0.03	0.02	0.03	0.02	0.02	0.14
Ca	0.10	0.11	0.11	0.11	0.11	0.10	0.10	0.10	0.11	0.10	0.11	0.11	0.11	0.09	0.17	0.11	0.11	0.07
Tot. cat.	8.001	8.005	8.016	8.018	8.018	8.020	8.014	8.014	8.019	8.011	8.018	8.003	8.038	8.076	8.006	7.998	7.997	8.002
Almandine	69.8	70.1	71.4	72.3	72.2	71.6	71.8	71.7	71.5	72.6	71.5	72.3	73.1	74.9	72.1	72.5	72.2	83.3
Spessartine	26.1	25.5	24.3	23.1	23.8	24.3	24.2	24.1	23.8	23.1	23.8	22.8	22.0	21.6	21.1	23.2	23.4	9.8
Grossular	2.0	2.6	3.6	3.8	3.5	3.6	3.3	3.5	3.7	3.5	3.7	3.7	3.9	3.0	3.4	2.8	3.1	1.9
Pyrope	0.6	0.6	0.7	0.8	0.5	0.6	0.7	0.7	1.0	0.9	1.0	1.1	1.0	0.5	1.2	0.7	0.7	4.6
Andradite	1.5	1.2													2.2	0.9	0.6	0.5
	100.0	100.0	100.0	100.0	100.0	100.0	100.0	100.0	100.0	100.0	100.0	100.0	100.0	100.0	100.0	100.0	100.0	100.0

Coyaguayma analyses from Caffe et al. (2012).
[a] Analyses from Viramonte et al. (1994) and Gauthier et al. (1994).

Table 2
Representative biotite, amphibole and alkali feldspar compositons.

Minerals	Biotite and biotite like Guanaco Formation tuffs					Coyaguayma				Amphibole Guanaco Formation tuffs		Alkali Feldspar	
Localities	Xibi-Xibi		Los Alisos			Ignimbrite				Los Alisos		Los Alisos	
Samples	Xi 9	Xi 13	Xi 13	Xi 13	DA 5-1	DA 5-2	DA 5-3	DA 5-4	PQ01-40p*	DA5-1	DA5-2	DA5-2	DA 5
SiO_2	38.87	36.74	39.80	39.24	36.59	36.18	34.68	36.06	32.89	40.45	39.98	39.97	68.83
TiO_2	0.98	1.66	1.30	1.62	1.21	1.56	4.35	1.31	1.33	1.94	2.08	2.11	–
Al_2O_3	19.73	19.39	18.94	18.04	16.86	17.70	15.99	17.85	19.75	12.01	11.85	12.02	19.07
Fe_2O_3										2.68	3.17	4.77	–
FeO	14.99	16.67	16.54	17.10	16.98	17.63	18.66	16.46	29.46	13.57	13.08	12.31	0.05
MnO	0.17	0.25	0.14	0.19	0.33	0.47	0.24	0.20	0.20	0.56	0.54	0.61	–
MgO	9.91	9.82	10.70	10.62	10.77	9.44	8.76	9.45	3.28	9.58	9.87	9.79	–
CaO	0.29	0.11	0.13	0.08	0.14	0.11	0.11	2.00	0.00	11.04	11.18	11.08	–
Na_2O	0.12	0.14	0.09	0.04	0.08	0.14	0.27	0.11	0.51	2.00	1.94	1.89	0.21
K_2O	5.49	6.28	5.92	7.24	6.33	9.11	9.60	8.62	8.77	1.56	1.63	1.62	11.02
H_2O^*	3.97	3.91	4.06	4.03	3.81	3.85	3.80	3.85	3.77	1.94	1.94	1.95	–
Total	94.51	94.96	97.62	98.19	93.10	96.19	96.46	95.91	99.96	97.33	97.26	98.12	99.18
#Mg	0.540	0.510	0.640	0.530	0.530	0.490	0.460	0.510	0.166	0.557	0.574	0.586	Ab 2.8 Or 97.2
									Caffe et al. (2012)				

Normalized to 100	Biotite and biotite like								Amphibole			
SiO_2	41.13	38.69	40.77	39.96	39.30	37.61	35.95	37.60	32.89	41.56	41.11	40.74
TiO_2	1.04	1.75	1.33	1.65	1.30	1.62	4.51	1.37	1.33	1.99	2.14	2.15
Al_2O_3	20.87	20.42	19.40	18.37	18.11	18.40	16.58	18.61	19.75	12.34	12.18	12.25
Fe_2O_3										2.75	3.26	4.86
FeO	15.86	17.55	16.94	17.42	18.24	18.33	19.34	17.16	29.46	13.94	13.45	12.55
MnO	0.18	0.26	0.14	0.19	0.35	0.49	0.25	0.21	0.20	0.58	0.56	0.62
MgO	10.49	10.34	10.96	10.82	11.57	9.81	9.08	9.85	3.28	9.84	10.15	9.98
CaO	0.30	0.12	0.13	0.08	0.15	0.11	0.11	2.09	0.00	11.34	11.49	11.29
Na_2O	0.13	0.15	0.09	0.04	0.09	0.15	0.28	0.11	0.51	2.05	1.99	1.93
K_2O	5.80	6.61	6.07	7.37	6.80	9.47	9.95	8.99	8.77	1.60	1.68	1.65
H_2O^*	4.20	4.11	4.16	4.10	4.09	4.00	3.94	4.02	3.77	1.99	1.99	1.99
	100.00	100.00	100.00	100.00	99.99	100.00	100.00	100.00	99.96	100.00	100.00	100.00
Original analyses	94.51	94.96	97.62	98.19	93.10	96.19	96.46	95.91	99.96	97.33	97.26	98.12

on the Mn-Mg-Fe^{2+} (spessartine-pyrope-almandine) triangular diagram in Fig. 4. The closest match for the MnO contents in the Guanaco/Ramada garnets in the Harangi et al. (2001) compilation are some type 4 garnets in xenoliths in Pannonia Basin andesites. The Guanaco Formation and Ramadas Volcanic Center garnets are also notable for having higher spessartine contents than the garnets (~9.8% spessartine; 4.3 wt% MnO) in the 11.3 Ma Puna Coyaguayma ignimbrite to the north (Fig. 1) described by Caffe et al. (2012). On the other hand, the spessartine contents in the Guanaco-Ramadas garnets are not as extreme as those in the garnets (Sp28-40) in the Ordovician Peñón Rosado Granite in the same tectonic belt in the Pampean ranges, some 500 km to the south (Dahlquist et al., 2007).

Other mineral grains in the tephra from the Xibi-Xibi and Los Alisos sections include sparse small flakes of brownish and pleochroic biotite, whose compositions are shown in Table 3. As the grains are small, some analyses have minor overlap effects. Even so, it is clear that these biotite compositions are significantly different from those in the Coyaguayma garnet-bearing rhyolite to the north (see Table 3). The main differences are higher Mg numbers (0.46–0.50 versus 0.16–0.17), lower wt% SiO_2 (38–41% versus ~33%) and lower wt% Na_2O (0.05–0.15 versus

Table 3
Major element analyses of glass shards in Guanaco Fm. tepras normalized to 100 wt%.

	Los Alisos section							Xibi-Xibi section						
Sample	DA5							Xi9					Xi13	
SiO_2	76.39	76.11	75.93	76.43	76.07	77.53	76.41	76.22	76.90	76.58	76.41	77.04	76.66	77.08
TiO_2	0.00	0.00	0.00	0.08	0.11	0.02	0.00	0.10	0.02	0.00	0.04	0.02	0.00	0.03
Al_2O_3	13.79	14.20	13.61	13.88	13.71	13.92	13.77	14.28	14.43	14.21	14.03	14.17	14.11	14.01
FeO	0.65	0.87	0.83	0.99	0.62	0.58	1.13	0.91	0.82	0.93	1.13	0.78	0.87	0.74
MnO	0.23	0.25	0.07	0.18	0.20	0.15	0.16	0.30	0.16	0.13	0.22	0.00	0.12	0.13
MgO	0.05	0.02	0.00	0.03	0.00	0.03	0.00	0.02	0.00	0.00	0.00	0.00	0.02	0.03
CaO	0.60	0.45	0.53	0.64	0.73	0.60	0.66	0.56	0.58	0.53	0.48	0.58	0.51	0.62
Na_2O	3.66	3.48	4.01	3.39	3.67	3.74	4.06	4.15	3.78	3.93	3.83	3.62	4.18	3.64
K_2O	4.35	4.39	4.77	4.35	4.81	3.36	3.72	3.42	3.28	3.55	3.59	3.75	3.53	3.63
$^{P}2^{O}5$	0.10	0.00	0.07	0.03	0.07	0.07	0.04	0.04	0.00	0.00	0.07	0.04	0.00	0.09
F	0.17	0.23	0.19	0.00	0.00	0.00	0.05	0.00	0.03	0.13	0.20	0.00	0.00	0.00
Cl	0.02	0.00	0.00	0.00	0.01	0.00	0.00	0.00	0.00	0.02	0.00	0.00	0.00	0.00
Original microprobe analyses totals														
	93.12	92.85	92.66	92.71	92.47	93.13	91.82	91.21	91.64	91.87	92.84	92.26	91.44	91.50
Originals oxide totals to indicate approximate degree of hydration of volcanic glass														
%	6.88	7.15	7.34	7.29	7.53	6.87	8.18	8.79	8.36	8.13	7.16	7.74	8.56	8.50

Table 4
Major and trace element analyses of Ramadas Center Volcanic Rocks and Guanacos Formation Distal Tephras.

	Ramadas Volcanic Center				Guanaco Formation											
	Obsidian	Obsidian	Pumice	Perlite	Xibi-Xibi								Los Alisos		Route 9 Metan	
Sample	RaOb1	RAOB	RaOb2	RaOb3	Xi1	Xi1glass	Xi2	Xi5	Xi8	Xi-9	Xi-12	Xi-18	DA-5	DA-6	R9 Met2	MN18
SiO_2	75.78	75.89	74.19	69.72	71.51	–	71.49	72.29	71.80	70.04	72.13	72.73	71.55	71.28	68.46	70.26
TiO_2	0.01	0.00	0.01	0.02	0.14	–	0.11	0.04	0.04	0.02	0.04	0.05	0.06	0.14	0.05	0.07
Al_2O_3	14.21	13.74	13.82	14.04	13.46	–	13.22	13.48	13.55	14.29	14.04	13.53	13.42	13.99	14.00	14.37
FeO	0.85	0.90	0.93	1.01	1.55	1.19	1.70	1.00	1.07	0.87	0.88	1.00	1.14	1.52	1.15	1.24
MnO	0.12	–	0.12	0.13	0.11	–	0.10	0.12	0.12	0.13	0.11	0.10	0.11	0.10	0.10	0.09
MgO	0.19	0.29	0.18	0.98	0.77	–	0.87	0.33	0.44	0.99	0.61	0.50	0.30	0.84	1.45	1.64
CaO	0.60	0.02	0.62	0.61	0.82	–	0.88	0.68	0.76	0.94	0.80	0.76	0.71	0.92	0.72	0.91
Na_2O	3.59	0.71	3.85	3.03	3.08	4.54	3.82	3.75	3.60	3.26	3.23	3.38	3.44	2.84	5.06	3.38
K_2O	4.72	3.72	4.27	4.60	3.30	–	3.19	3.76	3.66	2.65	3.66	3.73	4.14	3.78	2.80	2.79
P_2O_5	0.03	4.76	0.04	0.06	0.06	–	0.06	0.04	0.04	0.05	0.05	0.05	0.04	0.06	0.03	0.04
LOI	0.05	–	1.75	4.61	5.81	–	6.07	5.25	5.40	6.58	5.17	5.09	5.23	4.53	7.37	6.12
Total	100.16	100.03	99.78	98.81	100.62	–	101.51	100.74	100.47	99.83	100.71	100.93	100.15	99.99	101.19	100.91
Si normalized to	75.82	75.89	75.51	73.13	75.89	–	76.04	76.26	75.88	74.98	76.03	76.59	75.49	74.66	73.84	74.80
La	8.6	8.3	10.4	8.7	–	11.8	15.7	10.1	–	9.3	9.7	11.1	11.7	–	11.2	12.2
Ce	22.8	22.7	24.6	23.6	–	30.6	37.8	25.4	–	22.4	24	26.8	29.5	–	30.3	28.1
Nd	11.1	11.0	11.1	12	–	14.3	17.8	13.4	–	10.5	10.9	12.3	13.5	–	13.5	13.5
Sm	4.18	4.32	4.73	4.19	–	5.66	6.22	4.65	–	4.18	4.53	4.78	5.37	–	4.95	5.02
Eu	0.05	0.05	0.06	0.08	–	0.12	0.28	0.1	–	0.07	0.09	0.13	0.15	–	0.12	0.14
Tb	0.797	0.781	0.888	0.696	–	0.927	1.038	0.771	–	0.791	0.806	0.841	0.898	–	0.826	0.804
Yb	1.48	1.56	1.76	1.44	–	1.22	2.08	1.51	–	2.25	1.08	1.31	1.63	–	1.41	1.17
Lu	0.155	–	0.199	0.156	–	0.146	0.262	0.159	–	0.253	0.103	0.157	0.175	–	0.143	0.121
Y	23	–	24	23	26	–	26	24	24	29	24	24	29	27	21	26
Rb	370	–	367	349	282	–	277	346	337	243	320	326	327	294	266	264
Sr	See below				77	55	93	38	52	99	63	56	59	105	121	145
Ba	31	47	21	42	159	127	145	113	138	199	131	99	169	184	52	37
Cs	28.6	28.5	30.7	27.2	8.4	33.9	29.6	28.5	–	21.2	25.2	27.5	29.2	–	25.5	20.1
U	14.4	11.5	13.9	12.6	12.7	16.0	10.9	13.5	13.3	12.8	13.2	12.1	12.6	10	14.8	13.3
Th	10.4	8.0	13	10.3	10.7	9.6	11	10.3	10.8	12.1	10.3	9.4	8.6	11	8.7	10.1
Pb	60	–	38	39	43	–	39	41	39	39	36	36	–	–	156	–
Hf	2.3	2.2	2.4	2	4.7	2.6	3.6	2.6	2	2	3	3	2.9	2	2	2
Zr	29	–	29	29	83	–	72	44	41	47	40	53	50	72	45	60
Nb	41	–	42	41	36	–	37	42	42	44	40	41	31	29	42	44
Ta	3.85	4.00	4.22	3.78	4.62	4.62	4.37	3.92	–	3.59	3.79	3.89	4.04	–	4.59	3.89
Sc	4.9	4.6	5.3	5.2	9.8	6.3	7.5	5.3	–	4.9	5	5.5	5.8	–	6.4	5.5
Cr	150	5	1	50	21	4	11	3	32	15	13	5	5	35	19	22
Ni	4	0	2	5	8	0	8	2	4	4	3	3	7	8	4	6
Co	3	0	4	4	5	1	5	4	4	4	3	4	18	7	3	4
Sr ppm			6.4[a]				10[a]			8[a]						
$^{87}Sr/^{86}Sr$			0.726830				0.721500			0.723210						
$^{87}Sr/^{86}Sr_{int}$			0.711859				0.711996			0.711913						0.711922
$^{143}Nd/^{144}Nd$			0.512279				0.512279			0.512279						
$^{143}Nd/^{144}Nd_{int}$			0.512274				0.512274			0.512274						0.512274
Epsilon Nd initial			−6.98				−6.98			−6.98						

[a] Calculated Sr concentration - see text.

0.26–0.51) indicating they come from a more mafic source. They also differ from the Coyaguayma biotites in lacking inclusions of zircon, sillimanite or garnet. The Guanaco Fm. biotites are like those at Coyaguayma in having generally low wt% TiO_2 (<1.6%) and high wt% Al_2O_3 (18–20%). The exception is Los Alisos biotite DA5-3, which has ~36% SiO_2, 4.51% TiO_2, 16.6% Al_2O_3 and 0.28% Na_2O.

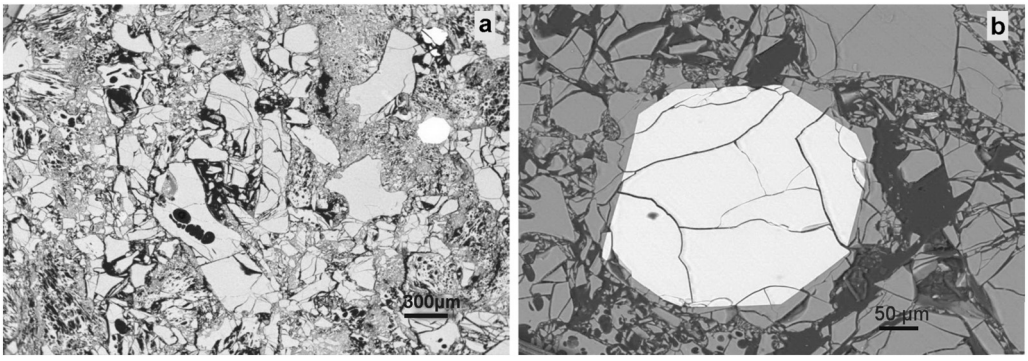

Fig. 3. Photomicrographs of thin sections in plane light of Guanaco Formation tuffs. (a) Texture of a vitroclastic tuff from the Xibi-Xibi section (sample Xi9) showing coexistence of vesicle-poor blocky glass shards and bubble wall shards in a fine-grained ash matrix. (b) Close-up of an euhedral garnet phenocryst surrounded by a glassy rim in a vitric tuff from the Alisos section (sample DA5). See Fig. 2 for sample locations.

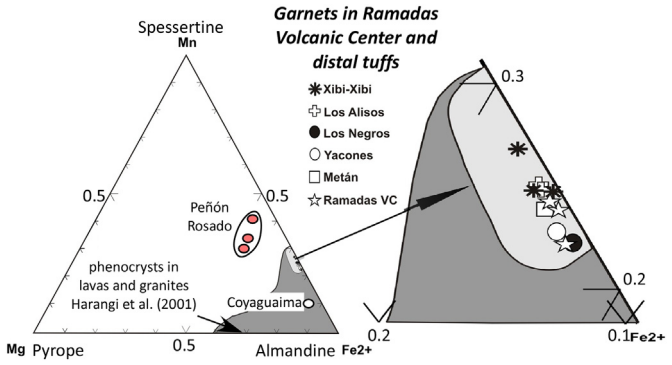

Fig. 4. Garnet compositions plotted as end-members on a triangular plot of cation percent Mg (pyrope)—Mn (spessartine)—Fe^{2+} (almandine) after Miller and Stoddard (1981). Garnet compositions are from Guanaco Formation tuffs along the Xibi-Xibi (asterisks) and Los Alisos (crosses) rivers (Table 1), Metán valley (square), Yacones (open circle) and Los Negros (filled circles) tuffs (Viramonte et al., 1994) and Ramadas Volcanic Center (stars) obsidian, perlite and pumice (Gauthier et al., 1994). Comparative garnet compositions from the northern Puna Coyaguayma Ignimbrite are from Caffe et al. (2012), the general field for garnets in the Ordovician Peñón Rosado granite in the Argentine Sierras Pampeanas is based on analyses in Dahlquist et al. (2007) and the global compilation of garnet compositions in volcanic and granitoid rocks is from Harangi et al. (2001). Figure on right shows a blow-up of the Fe^{+2} corner (region in dark gray) with garnet composition from Xibi-Xibi, Los Alisos and R9Met2 sections and Ramadas Volcanic Center.

The only other silicate minerals in the Guanaco Fm. tuffs are rare green to greenish-yellow subhedral amphiboles in the Los Alisos tuff whose compositions are shown in Table 2. As with the biotite, the grains are small and the analyses can overlap the matrix. Nevertheless, the overall compositions are clear. Using the classification of Leake et al. (1997), the amphiboles are Mg-hastingsite with Mg# = 0.51–0.40, Ca > 1.5; (Na + K) > 0.5; Ti > 0.5and Si = 6. Following Ridolfi et al. (2010), the compositions in Los Alisos sample DA5-1 & DA5-2 suggest a mafic igneous origin with temperature near 940 ± 20 °C, a pressure of ~440 ± 111 MPa (depth of ~16–17 km), a log fO_2 of −11 (near NNO buffer) and a water content of ~5.5 ± 1.9%. The compositions are out of equilibrium with the garnets, supporting the interpretation that the grains are xenocrysts.

3.2. Major and trace element compositions of the glass shards and tephras of the Guanaco Formation and the pumice, obsidian and perlite from the Ramadas Volcanic Center

Microprobe analyses of the major element compositions of the juvenile micro-pumice fragments and glass shards (grain size >125 μm) in samples from the Guanaco Formation in the Xibi-Xibi and Los Alisos profiles are shown in Table 3. When normalized to 100%, the analyses show relatively homogeneous rhyolitic compositions with 76–77.5% wt% SiO_2, 3.4–4.2 wt% Na_2O, 3.3–4.8 wt% K_2O, 0.6–1.1 wt% FeO and 0.02–0.12 wt% TiO_2. Plots of wt% SiO_2 versus Al_2O_3 and K_2O versus CaO in Fig. 5 for the glass shards in Xibi-Xibi samples Xi-9 and Xi-13 and Los Alisos sample Da-5 show the relatively small compositional range within and between samples. In detail, the Los Alisos glass shards have slightly lower wt% Al_2O_3 and higher wt% K_2O content than those from the Xibi-Xibi profile.

In comparison, Table 4 lists the XRF whole rock major and trace element analyses of an assortment of bulk tephra samples from the Guanaco Formation tuffs in the Los Alisos and Xibi-Xibi profiles and typical obsidian, pumice and perlite samples from the Ramadas Volcanic Center. When calculated on an anhydrous basis, the whole rock analyses of the Ramadas Volcanic Center samples are compositionally similar to the individual shard analyses in showing a fairly homogeneous range of peraluminous (A/CNK = 1.2–1.4) rhyolitic compositions with 74.0–75.9 wt% SiO_2, 3.1–4.7 wt% Na_2O, 2.9–4.4% wt. K_2O and 0.01–0.14% wt% TiO_2. As the bulk tephra whole rock analyses have LOI contents up to ~6.5% (Tables 3 & 4), a plot of normalized SiO_2 concentration versus Zr/TiO_2 on the discrimination diagram of Winchester and Floyd (1977) confirms that both the Guanaco Formation tuffs and Ramadas Volcanic Center samples have rhyodacitic to rhyolitic compositions (Fig. 6).

Further, comparisons of the anhydrous-based glass shard analyses in Fig. 4 with those of the anhydrous-based bulk tephra sample show there is a virtual overlap of compositions in sample DA5 and a greater, but still small difference between the glass shards and bulk tephra of sample Xi-9. The same small differences in Al and K concentration in the glass shard compositions between Xi-9 and DA5 mentioned above occur in the analyses of the whole rock tephra. In accord with the tephra being phenocryst-poor, the bulk tephra compositions of the primary ashfall deposits seem to have been little modified by loss or concentration of phenocrysts or xenocrysts during atmospheric transport. As such, the whole rock analyses in Tables 3 and 4 can be used to correlate tephra layers in the Guanaco Formation of the Rio Grande of Jujuy and Metán valleys.

From a classification perspective, the tephra and Ramadas Volcanic Center analyses plot in the field of A-type granites near the I-type boundary on silicic rock discrimination diagrams. Fe * O/(Fe * O + MgO) ratios (Fe-indices) of ~1 at 76.6–77.5 wt% SiO_2 for the glass shards (Table 3) and from 0.48–0.93 at 72.6–75.9 wt% SiO_2 for the whole rock tephra (Table 4) fall in the field of ferroan volcanic rocks in the classification of Frost et al. (2016). Ferroan signatures like these are generally associated with reducing and relatively dry conditions. As with other strongly peraluminous ferroan Si-rich ignimbrites in the Puna like the Coyaguayma Ignimbrite (Caffe et al., 2012), Tocomar

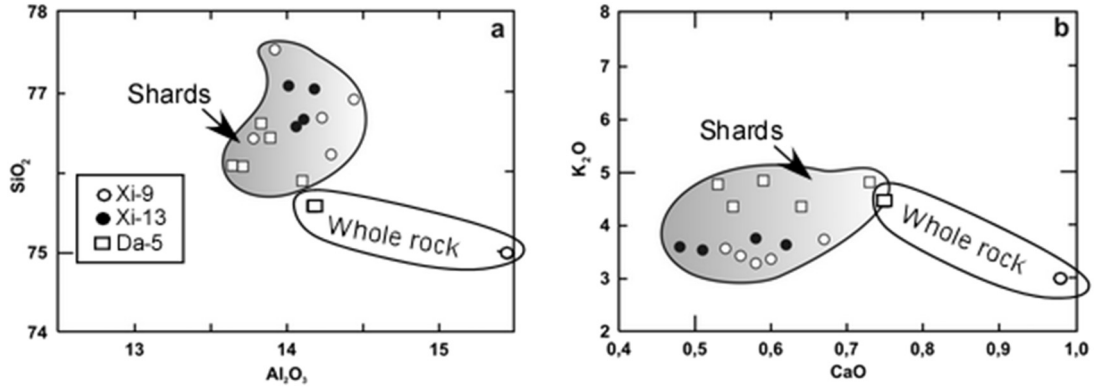

Fig. 5. Plots of wt% SiO_2 versus Al_2O_3 and K_2O versus CaO for microprobe analyzes of Guanaco Formation glass shards normalized to 100% from Table 3. Analyses are for Xibi-Xibi samples Xi-9 - open circles; Xi-13 - circles and the Alisos sample DA-5 (squares). Analyses of whole rock powders of samples DA5 (square with point) and Xi9 (circle with point) from Table 4 are shown for comparison. Not the close match between the shard and whole rock analyses of sample Da5. See discussion in text.

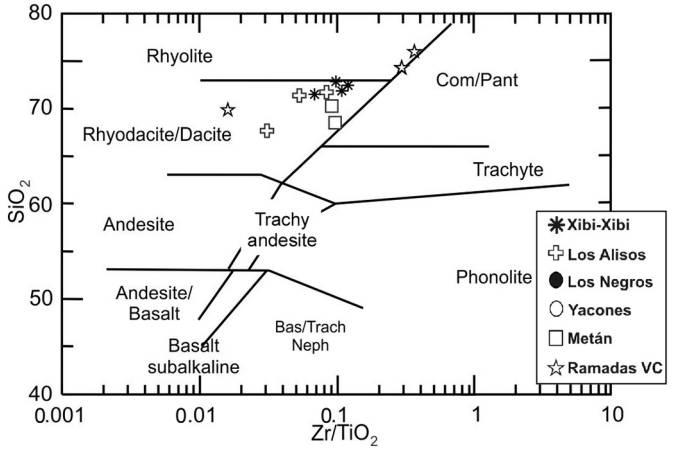

Fig. 6. Plot of wt% SiO_2 versus Zr in ppm/wt% TiO_2 from Winchester and Floyd (1977) for whole rock analyses of tuff samples from the Guanaco Formation Xibi-Xibi (asterisks), Alisos (crosses) and Metán (square) profiles and obsidian, perlite and pumice samples (stars) from the Ramada Volcanic Center confirming their overlapping rhyodacitic to rhyolitic compositions.

rhyolite (Petrinovic et al., 2006) and Botijuela-Minas rhyolites in the Antofalla region (Richards et al., 2006), the shards have low Sr, Ba, Zr and LREE and high Rb, Nb and Ta concentrations (Table 4; Figs. 7 & 8).

Representative REE and other trace element data from Guanaco Formation tuffs are shown on chondrite and primitive mantle normalized trace element plots in Fig. 7. The REE diagrams (Fig. 7a & b) show slight light REE enrichment (La/Yb = 6.7–10.4) with La/Sm ratios of 2.2–2.5, large negative Eu anomalies (Eu/Eu* = 0.07–0.14) and relatively high Sm/Yb ratios ~3.0–4.2 that require heavy REE retention in residual hornblende and garnet in the source. The primitive mantle normalized patterns (Fig. 7d & e) show strong enrichments in Cs, Rb, U and Pb, moderate enrichments in Th, Ta and Nb, moderate depletions in Sr and Zr and strong depletions in Ti and Eu relative to the LREE that lead to low Ba/La (most 10–14), Ba/Ta (24–55) and very low La/Ta (3–4) ratios. The positive spikes in Pb, Th and U indicate continental crustal components and negative spikes in Ba, Sr and Eu reflect plagioclase and sanidine fractionation.

The analyses of the Guanaco Fm. tuffs can be compared with those of the garnetiferous obsidian rhyolite (RaOb1), perlite (RaOb2) and pumice (RaOb3) in the Corte Blanco tuff from the Ramadas Volcanic Center in Table 4 and Fig. 7c and f. The REE and extended trace element plots of the Ramadas Volcanic Center samples highlight the marked overlap in the concentrations of most elements with the Guanaco Fm. tuffs. Minor differences in Eu, Sr, Ba and Sr are best explained by variable amounts of sanidine and differences in the heavy REEs by variable amounts of garnet. In detail, the Ramadas Volcanic Center obsidian and perlite samples have the largest Eu and Sr anomalies reflecting a greater feldspar (sanidine) loss. Lower Hf and Zr contents in the Ramadas sample could reflect more zircon loss.

4. Age of the Guanaco Formation Tephras and the Ramadas Volcanic Center

New laser step heating $^{40}Ar/^{39}Ar$ ages on glasses from three tuffs in the Guanaco Fm. in the Xibi-Xibi profile are shown in Table 5 with analytical details in Appendix 1. Samples from the Xibi-Xibi section dated in the Geochronology Laboratory, National Taiwan University using the techniques described by Lo et al. (2002) yielded plateau ages of 6.1 ± 0.2 Ma for tuff sample Xi-16 from the upper part of the section and 7.0 ± 0.6 Ma for tuff sample (XI-9) from the lower part (Fig. 2; Table 5). These ages overlap within error near 6.3 to 6.4 Ma. A third sample Xi-8 from just below Xi-9 dated at the Geochronology Laboratory at the University of Alaska Fairbanks using the techniques in Layer et al. (1987) yielded an isochron age of 5.4 ± 0.5 Ma, which is within error of the 6.1 ± 0.2 Ma age of sample Xi-16. The same sample also yielded a more poorly contained weighted plateau age of 4.2 ± 1.82 Ma (upper limit is 6.02 Ma).

In comparison, a whole rock K/Ar age of 8.73 ± 0.25 Ma for the Ramadas Volcanic Center event was suggested by Del Papa et al. (1993) and Viramonte et al. (1994) based on the mean K/Ar ages of a Ramadas Volcanic Center obsidian and a pumice from a medial facies tuff some 20 km to the east. Subsequently, Petrinovic et al. (1999) constrained the age of a medial pyroclastic facies in the Corte Blanco Tuff in a profile ~20 km south of the Ramadas Volcanic Center near the El Morro Center to be between the Ar/Ar biotite ages of 7.4 ± 0.3 Ma for the Toba I ignimbrite and 6.2 ± 0.3 Ma for the El Morro II Ignimbrite. More recently, a fission track age of 6.63 ± 0.28 Ma on an obsidian sample from the Ramadas Volcanic Center from Bigazzi (2004) overlaps the range of errors in the Ar/Ar ages of the Guanaco Formation tuffs.

Considering the difficulties of dating glass samples and taking into account the errors, the measurements are in accord with an eruption or eruptions between 7.0 ± 0.6 Ma and 6.1 ± 0.2 Ma as would be consistent with multiple tephra layers. Given the uncertainties, the most likely eruption age for the Guanaco Formation garnet-bearing tuffs is between 6.1 and 6.3 Ma. This age is in line with the vertebrate gliptodontoideo fossils (Fig. 2) found near the top of the ashes in the Xibi-Xibi section being in the Huayquerian "stage" (Arias et al., 1978), which is considered to late Miocene in age between 8 and 5 Ma (see Schmidt et al., 2018).

5. Revised Sr and Nd initial isotopic ratios for the Ramadas Volcanic Center

$^{87}Sr/^{86}Sr$ and $^{143}Nd/^{144}Nd$ isotopic ratios for samples from the Ramada Volcanic Center obsidian, pumice and perlite in the Corte Blanco tuff have previously been published in Viramonte et al. (1994, 2007). A long-standing problem in using these analyses in petrologic modeling is that calculating their initial $^{87}Sr/^{86}Sr$ ratios has been elusive due to the combined uncertainty in their age and the analytical uncertainty in their extremely low Sr concentrations. Here, we recalculate both their initial $^{87}Sr/^{86}Sr$ ratios and Sr concentrations using the following conditions: a) the eruption of the Ramadas Volcanic Center occurred at ~6.3 Ma based on the new age constraints discussed above, b) the assumption that the initial $^{87}Sr/^{86}Sr$ isotopic ratios for all three samples should be similar as they erupted at the same time from the same source, and c) their Rb concentrations are those reported in Table 4. Using these conditions, the recalculated Sr concentrations in Table 4 for the three samples from the Corte Blanco tuff are respectively 6.4, 10 and 8 ppm with an average recalculated $^{87}Sr/^{86}Sr$ initial ratio of 0.71192 at an average initial $^{143}Nd/^{144}Nd$ ratio of 0.512274 or an εNd of −7.0 (see Table 4). As illustrated in Fig. 9, the recalculated initial $^{87}Sr/^{86}Sr$ ratio are only slightly higher than those for the nearby late Miocene Aguas Calientes Ignimbrite, which should have a generally similar crustal contaminant (Matteini et al., 2002a).

6. Discussion: tephras as chronostratigraphic markers and source implications for the origin of the garnet-bearing Ramadas Volcanic Center magmas

6.1. Volcanic implications

A number of lines of evidence link the garnet-bearing tuffs in the Guanaco Formation in the Rio Grande of Jujuy and Metán Valleys to the Ramadas Volcanic Center, some 100 to 200 km to the west. The first and strongest indicator is the nearly identical composition of the near euhedral garnet phenocrysts ($Alm_{70-72}Sps_{22-26}Grs_{2-4}Prp_{5-1}$) in the Guanaco Formation tuffs (Table 2) to those in the Ramadas Volcanic Center rhyolite, obsidian and pumice analyzed by Viramonte et al. (1984) and Gauthier et al. (1994). These garnet compositions are also

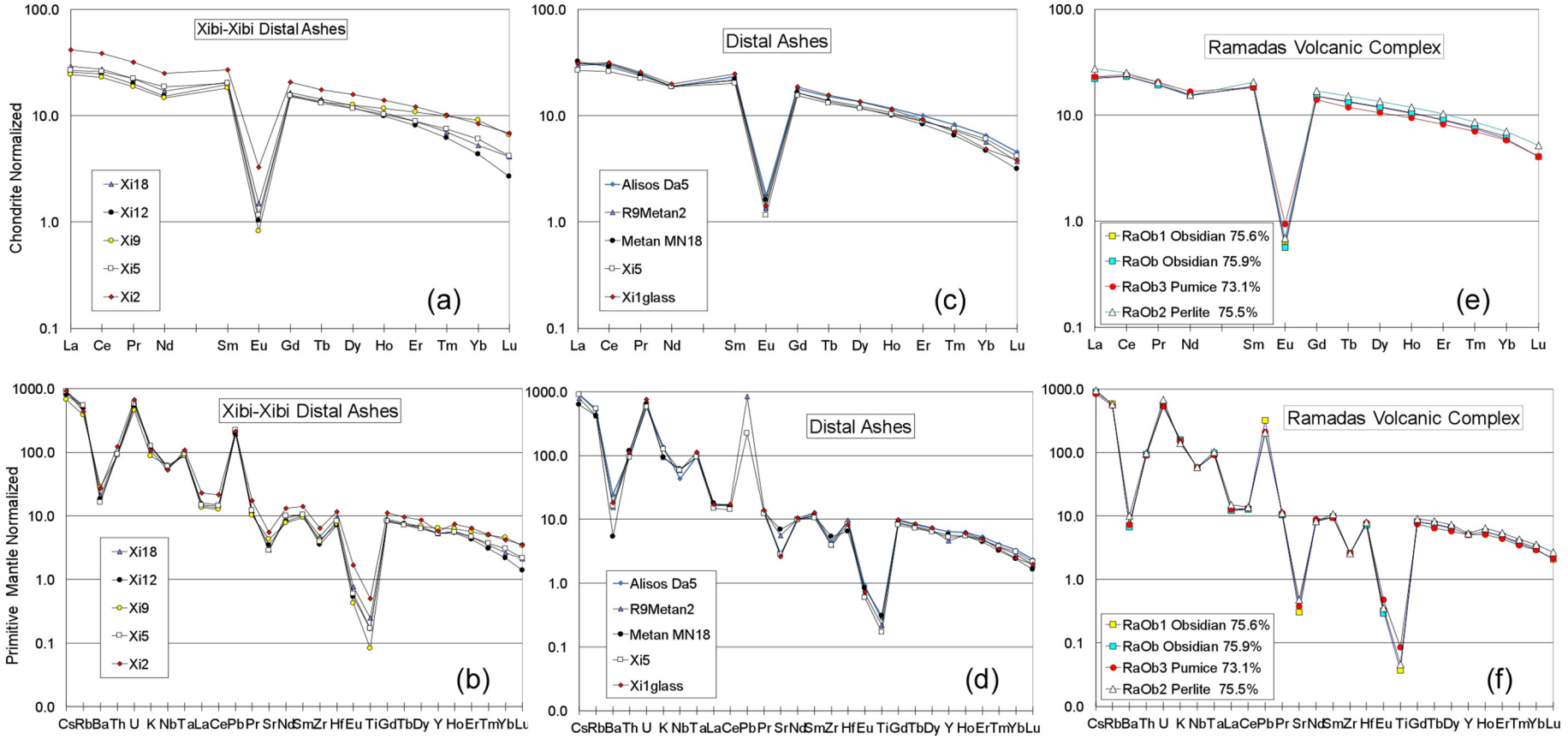

Fig. 7. Chondrite and primitive earth normalized trace element diagrams for whole rock samples of Guanaco Formation distal ashes from the Xibi-Xibi (a & b) and other (c & d) profiles compared to those from samples of rhyolitic obsidian, pumice and perlite samples from the Ramada Volcanic Center (e & f). Data are from Table 4 and normalization values are from Sun and McDonough (1989). See text for discussion.

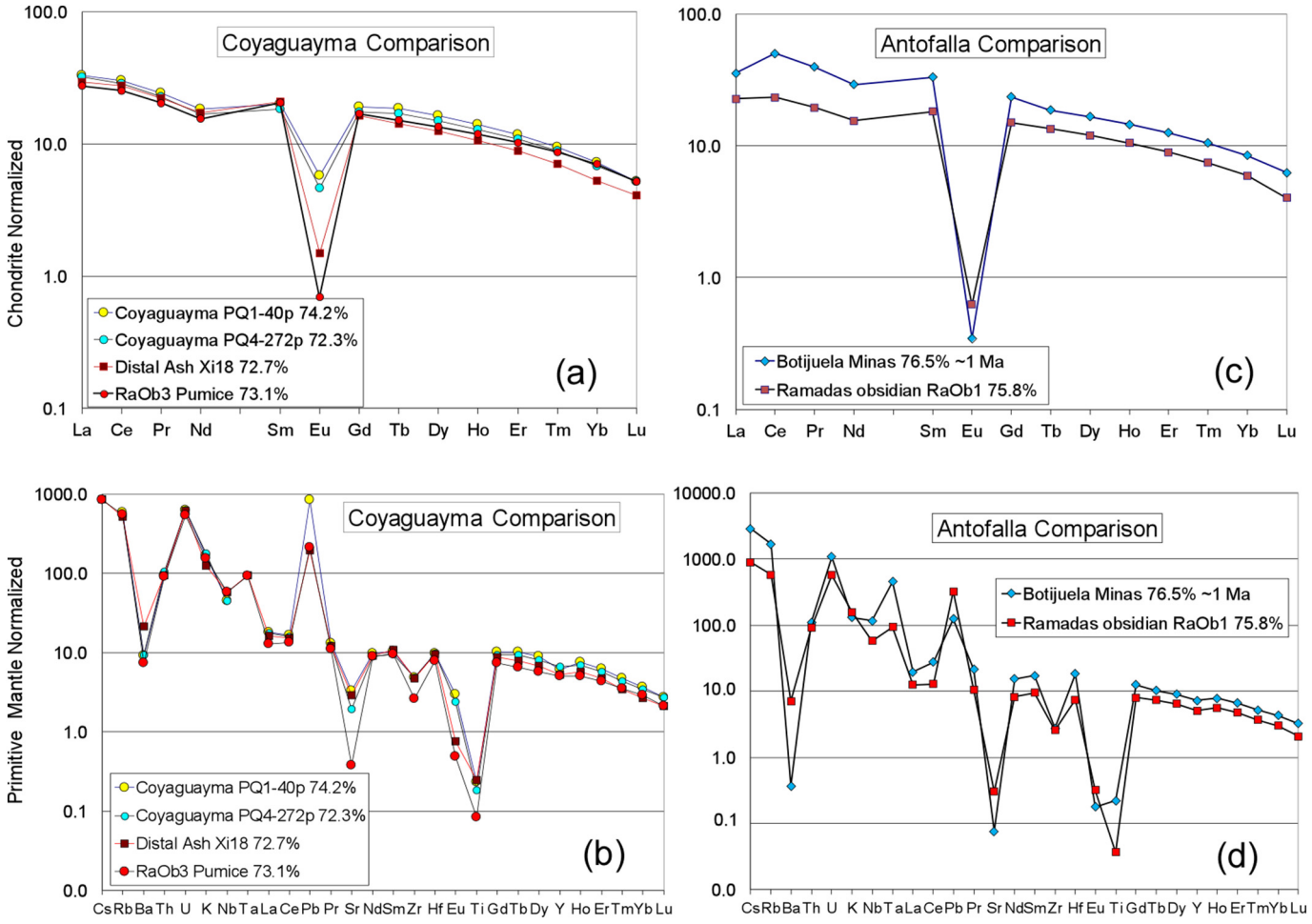

Fig. 8. Chondrite and primitive earth normalized trace element diagrams comparing Xibi-Xibi distal ashes and Ramada Volcanic Center rhyolites with Spessartine-rich garnet-bearing rhyolites from the Coyaguayma ignimbrite (data from Caffe et al., 2012) and Botijuela Obsidian dome (data from Richards et al., 2006). Normalization as in Fig. 7. See text for discussion.

like those in the Guanaco Formation tuffs in the Lerma and Metán valleys reported in Del Papa et al. (1993) and Viramonte et al. (1994). The second is that the $^{40}Ar/^{39}Ar$ ages of the Guanaco Formation tuffs in the Xibi-Xibi profile are within error of the ages suggested for the Ramadas Volcanic Center and its medial pyroclastic facies. A third is that the Guanaco Formation tephras show overlapping whole rock major element and strong trace element similarities to the pyroclastic rocks and rhyolitic dome of the Ramadas Volcanic Center (Table 4; Figs. 6 and 7). As shown in Fig. 7, trace element similarities include similar enrichments in Ta, Nb and Th relative to the LREE, very low Ba/La, Ba/Ta, La/Ta and Zr/Nb ratios, positive spikes in Th and U, relatively flat light REE patterns (La/Sm ratios ~2–2.5) with high Sm/Yb ratios (~2.8–4.0), that require retention of heavy REEs in hornblende and garnet in the source and large negative Eu anomalies ($Eu/Eu^* = 0.07–0.14$) requiring plagioclase fractionation.

Importantly, the garnet-bearing Guanaco Formation tephras also have similar garnet phenocrysts and compatible ages with the medial pyroclastic garnetiferous facies exposed 15–20 km to the east of the eruptive center of the Ramadas Volcanic Center (Viramonte et al., 1994; Tait, 2004). As such, the distribution of the tephra in the Guanaco Formation sections confirms the extension of tephra dispersion from the Ramadas Volcanic Center through the Corte Blanco to the Xibi-Xibi River and Alisos localities as well as to the southeast through the Valley of Lerma to the Metán locality (Fig. 1). This distribution pattern is in accord with the dispersal pattern proposed by Viramonte et al. (1994) and Tait (2004).

Further, the diverse vesicularity of the juvenile clasts in the Guanaco Formation tephra samples in the Los Alisos and Xibi-Xibi and Metán profiles suggests a mechanism for their generation. On the one hand, tube to cellular pumice fragments are common in plinian phase

Table 5
Ar/Ar ages of Glass from the Guanaco Fm. Xi-Xi section tuffs. See Appendix 1 for additional information, ages used in text are in bold. Geochronology Laboratory National Taiwan University.

Sample	Plateau age	Error	MSWD	Intergrated age	Error	Isochron age	
Xi-16	**6.1**	**± 0.2**	**0.36**	7.5	± 0.3	5.0	±1
Xi-9	**7.0**	**± 0.6**	**1.53**	7.2	± 0.5	6.0	±2

LP6a Biotite Standard Age = 128.4 ± 0.8
Ma J-value = 0.0036115 ± 0.0000253

Geochronology Laboratory University of Alaska Fairbanks
Plateau age based on weighted average

				Isochron age	
Xi-8	4.2	±1.82	2.65	**5.4**	**±0.5**

TCR-2 Standard Age = 28.619 Ma
Weighted average of J from standards = 8.314e-05 ± 2.212e−07

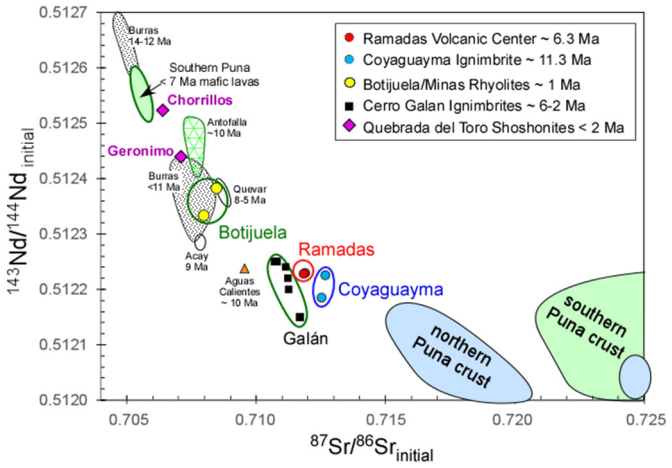

Fig. 9. Plot of initial $^{143}Nd/^{144}Nd$ and $^{87}Sr/^{86}Sr$ ratio for Ramadas, Coyaguayma, and Botijuela garnet-bearing rhyolites and comparative samples from the Puna. Initial isotopic ratios for the Ramadas Volcanic Center and Botijuela region samples from Table 4 are as recalculated from analytical data in Viramonte et al. (1994, 2007) and Richards et al. (2006) following discussion in the text. Data for the Coyaguayma ignimbrite are from Caffe et al. (2012), Cerro Galán ignimbrites from Francis et al. (1989), Quebrada del Toro shoshonites and Southern Puna mafic lavas from Kay et al. (2010) and other samples as in or compiled by Petrinovic et al. (1999), Matteini et al. (2002a), Mazzuoli et al. (2008) and Kay et al. (2010). Fields for northern and southern Puna bulk crust are based on compilation in Caffe et al. (2012). Garnet-bearing rhyolites are all consistent with being ~50–50 mixtures of mantle and crustal derived magmas as discussed in text.

eruptions and their presence in the distal facies is consistent with the model of Tait et al. (2009). At the same time, the co-existence of these fragments with a similar proportion of blocky glass shards with very low vesicularity in the same layer is best explained if the Guanaco Formation tuffs represent the opening of the vent that produced the initial pyroclastic surge deposits. In this case, the blocky fragments did not form due to large amounts of volatile exsolution, but instead are products of phreatomagmatic fragmentation in accord with the textural criteria in Wohletz (1983). Thus in the Ramadas Volcanic Center evolution scheme of Tait et al. (2009), the Guanaco Fm. tuffs reflect an initial vent opening associated with a series of pulsating phreatic magmatic surges as seen in Fig. 10a before the initiation of the Plinian stage seen in Fig. 10b. The volcanic deposits associated with the opening and initial Plinian phase are then those recognized by Tait (2004) as forming the lowest unit of the Corte Blanco tuff, some 20 km from the vent.

6.2. Petrologic implications: mixing of mantle and Mn-rich crustal melts and crystallization of garnet from a rhyolite melt extracted from a crystal mush

The geochemical analyses and recalculated $^{87}Sr/^{86}Sr$ and $^{143}Nd/^{144}Nd$ initial ratios of the Ramadas and Guanaco Formation tuffs in Table 4 allow a refined interpretation of their magmatic origin and permit comparisons with the ~6–2 Ma Cerro Galan Ignimbrites to the south and the other spessartine garnet-bearing silicic Puna volcanic rocks in Fig. 1 including the Coyaguayma Ignimbrite (Caffe et al., 2012) to the north and the Botijuela obsidian west of the Salar de Antofalla (Richards et al., 2006). For comparison, the trace elements of the Coyaguayma Ignimbrite and Botijuela obsidian are plotted in Fig. 8, and the initial Sr and Nd isotopic ratios of all of the comparative centers in the Puna are shown in Fig. 9.

As seen in Fig. 9, the initial ratios of the Ramadas rhyolites are only slightly higher in $^{87}Sr/^{86}Sr$ than those of the 6 to 2 Ma Cerro Galan ignimbrites (Francis et al., 1989) for which Kay et al. (2010, 2011) calculated a nearly 50:50 crustal-mantle mixing ratio based on O-Sr-Nd isotopes and trace element modeling. In those models, the mantle-derived end-member was assigned an $^{87}Sr/^{86}Sr$ ratio of 0.7055 and a $^{143}Nd/^{144}Nd$ ratio of 0.5126 based on the analyses of the <7 Ma southern Puna mafic lavas (Fig. 9). The resulting crustal contaminant required Nd and Sr isotopic ratios in the range estimated for the Puna crust (Fig. 9). In comparison, the <2 Ma Chorrillos absarokite (52.12% SiO_2; 6.88% MgO; ~380 ppm Cr) in the Quebrada del Toro shoshonitic suite, which erupted 10 km south of the Ramadas Volcanic Center (Fig. 1), has $^{87}Sr/^{86}Sr$ (0.706333) and $^{143}Nd/^{144}Nd$ (0.512519) ratios that are only slightly more enriched than those of the southern Puna mafic lavas (see Kay et al., 1994). Supporting evidence for a role for a shoshonitic suite mafic magma comes from the Mg-rich biotite and Mg-hastingsite xenocrysts in the Guanaco tuffs (see below). As such, in analogy with the Cerro Galan ignimbrites, near 50:50 mixtures of a primitive shoshonitic series mafic magma with melts of the Puna crust might produce the Ramadas magmas.

As noted by previous investigators (Petrinovic et al., 1999; Matteini et al., 2002a and 2002b; Mazzuoli et al., 2008; Kay et al., 2010), compiled

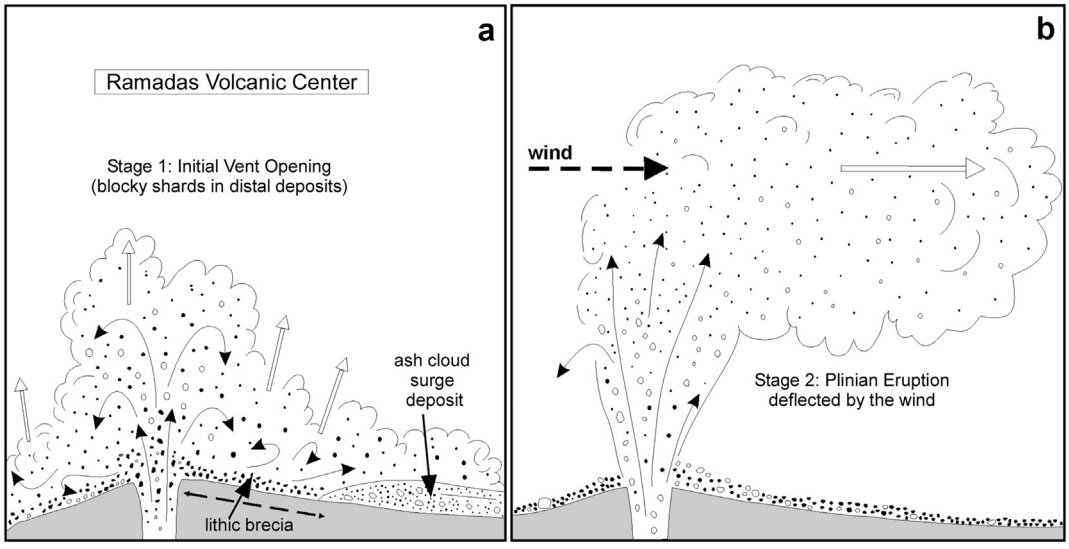

Fig. 10. Schematic model for the evolution of the plinian phase of the Ramadas Volcanic Center eruption. (a) Initial opening of the vent with production of a lithic breccia deposit and ash cloud surge deposit producing blocky shards. (b) This initial opening is immediately followed by a Plinian eruption in which ash and pumice with both blocky and bubble wall shards are deflected by eastward directed winds. In the sketches, the black circles represent the lithic fragments and the open circles represent the tube to cellular pumice fragments and blocky shards.

isotopic data for the region along the Olacapato-El Toro lineament near the Ramadas Volcanic Center show an increase in $^{87}Sr/^{86}Sr$ and a decrease in $^{143}Nd/^{144}Nd$ ratios with age in samples at a similar stage of evolution. This pattern can generally be correlated with incorporation of an increasingly more radiogenic crustal component in the magma source in response to crustal thickening and an increasingly enriched mantle in response to lithospheric removal (e.g., delamination; Kay et al., 1994; Kay et al., 2010). The combination of incorporating the Neoproterozoic-Eocambrian Puncoviscana greywackes into the magma in the crust and the enriching of the mantle source that lead to the formation of the shoshonitic magmas provide the ingredients to set the stage for producing the Ramadas rhyolites.

Further constraints on the origin of the Ramadas Volcanic Center magmas and Guanaco tuffs come from comparisons with the chemistry and mineralogy of the peraluminous Coyaguayma Ignimbrite investigated by Caffe et al. (2012). Some of the distinctive geochemical similarities and differences with the Ramadas tuffs can be seen in the REE and primitive mantle normalized trace element patterns in Fig. 8a and b. The most striking similarities include large negative Eu and Sr anomalies that require feldspar fractionation, steep REE patterns that require retention of HREE in residual garnet and amphibole, positive Pb anomalies requiring crustal contaminants and low Zr, Th and LREE requiring monazite and zircon removal. At the same time, the most notable differences from the Coyaguayma tuffs include much larger negative Eu and Sr anomalies, slightly steeper REE patterns, more pronounced negative Ti anomaly and less pronounced positive Pb spike that complement the slightly less enriched Sr and Nd isotopic ratios in the Ramadas tuffs (Fig. 9).

An important factor in interpreting some of these similarities and differences is that the Ramadas tuffs are almost aphyric except for a small amount of garnet consistent with crystallization from a residual melt after extreme fractionation of the hybrid magma in a mush zone. The lower Sr and Ba concentrations and larger negative Eu anomalies of the Ramadas tuffs imply more feldspar fractionation after assimilation. These differences are consistent with more crystallization of alkali and plagioclase feldspar, garnet, biotite and titanomagnetite from the Ramadas magma before extraction and eruption of the Ramadas tuff than before the eruption of the Coyaguayma Ignimbrite.

Of relevance to the Ramadas tuffs, Caffe et al. (2012) presented a major element and Rb, Ba, Sr and Y model for crystallizing the Coyaguayma ignimbrite from a dacitic magma (69.7% SiO_2), which is comprised of 70% of the ~4 Ma calc-alkaline Atana ignimbrite west of Coyaguayma and 30% of the strongly peraluminous ~7 Ma Morococala ignimbrite in Bolivia. Their least squares model shows the Coyaguayma pumice can be matched by ~70% equilibrium crystallization of 36% plagioclase, 29% quartz, 25% sanidine, 1% magnetite, 9% biotite and 0.6% apatite. They also present a fractional crystallization partial melting model showing that the average Argentine Puna metapelitic gneiss of Lucassen et al. (2001) produces the best match for the composition of the Coyaguayma ignimbrite and make the comment that their melting model cannot match the higher Rb/Sr and Rb/Ba ratios of the Ramadas rhyolites. Overall their source components are broadly consistent with a similar model for the Ramadas rhyolite with the differences being best explained by more K-feldspar and plagioclase retention in the crustal magma chamber at depth in line with the larger Eu anomaly and more extreme Ba and Sr anomalies (Fig. 8) and some regional differences in the mantle and crustal components.

The other spessartine-garnet bearing rhyolite is the ~1 Ma Botijuela rhyolitic obsidian dome west of the Cerro Galan caldera (Fig. 1). The age-corrected initial $^{87}Sr/^{86}Sr$ and $^{143}Nd/^{144}Nd$ ratios for these rhyolites, which are calculated from the measured values in Richards et al. (2006), are lower in $^{87}Sr/^{86}Sr$ (~0.7083) and higher in $^{143}Nd/^{144}Nd$ (~0.51235) than the ratios of the garnet-bearing Ramadas tuffs as is consistent with a less radiogenic basement west of the Salar de Antofalla than under Cerro Galan, the Ramadas Volcanic Center or the Coyaguayma ignimbrite.

7. Crystallization conditions

The crystallization conditions for the Ramadas rhyolitic magmas can be partially constrained by the compositions of the garnet and amphibole in Tables 2 and 3. Particularly, wt% MnO in the garnet can be used as an indicator of pressure. Early experimental work by Green (1977) showed that higher wt% MnO allowed garnet to stabilize at shallower depths and that garnets with >10 wt% MnO could crystallize from silicic liquids at pressures of 5 kbar or less. As the Ramadas garnets have ~10% wt% MnO (Table 2), they could have crystallized at depths of ~15 to 12 km. The subsequent experiments of Green (1992) showed that as pressures decreased, wt% MnO could increase with wt% CaO remaining relatively high (>4%). This, however, is not the case in the Ramadas garnets as wt% CaO are <1.5% suggesting an S-type crustal component in accord with Table 1 in Harangi et al. (2001),which shows that garnets in peraluminous granites often have lower wt% CaO at the same wt% MnO.

Furthermore, as has been observed in other silicic magmas with Mn rich garnets (see Harangi et al., 2001), tschermakitic magnesiohastingsite or pargasitic amphibole compositions like those in the Guanaco tuffs (see Table 3) commonly occur as mafic phenocrysts or xenocrysts in garnet-bearing tuffs. The high Al, Ti, Na and K in these amphiboles indicate that they crystallized at high temperatures and pressures. Using the Ridolfi et al. (2010) calibration discussed above, the amphibole compositions in Los Alisos sample DA5-1 & DA5-2 permit a temperature near 940 ± 20 °C, a pressure of ~440 ± 111 MPa (depth of ~16–17 km), a log fO_2 of −11 near the NNO buffer and a water content of ~5.5 ± 1.9% in accord with the amphiboles being xenocrysts from a mantle-derived shoshonitic mafic magma that mixed with a crustal melt. The physical conditions are consistent with a mid-crustal magma chamber in which mantle-derived basaltic melts mixed with crustal melts like those might be derived from melts of the Neoproterozoic-Eocambrian Puncoviscana Fm. greywackes, which underlie the Ramadas Volcanic Center.

Biotite compositions in garnet-bearing magmatic rocks vary with the composition of the magma, with those in the rhyolites often having lower Mg numbers (29–40) and being less K_2O-rich (8.1–8.7%) than those in more mafic rocks. In contrast, the biotite and pseudo-biotite analyses in Table 2 for the Guanaco tuff from the Ramadas Volcanic Center are more Mg-rich (up to 10% MgO; Mg# 49–64) than either those in the Coyaguayma ignimbrites (~3% MgO; Mg# 16) or those typically found in garnet-bearing volcanic rocks suggesting they are xenocrystic. A possibility in explaining their relatively Mg-rich compositions is that they reflect reaction of phlogopite crystals derived from shoshonitic magmas with the rhyolites in the Ramadas mush zone. Such phlogopite-bearing (Mg# 70–90) crystals occur in the nearby Chorrillos and San Geronimo shoshonitic series flows that erupted along the Olacapato-El Toro lineament in the Quaternary (see Déruelle, 1991). The possible presence of mafic and possibly shoshonitic series magmas at depth at the time of the Ramadas eruption at 6.3 Ma is consistent with the appearance of mafic volcanism at ~7–6 Ma just to the north (e.g., Maro et al., 2017) and south of the Quebrada del Toro (e.g., Kay et al., 1994).

The petrography of the Ramadas rhyolite shows the only primary liquidus phenocryst is garnet. As such, the trace element evidence for residual feldspar, garnet, biotite and titanomagnetite is consistent with extraction of a rhyolite melt from a crystal mush at mid-crustal depths that then crystallized spessartine-rich garnet upon ascent. In line with studies of the Coyaguayma ignimbrite (Caffe et al., 2012) and the evidence above, the pre-eruption crystallization of the rhyolite segregated from the mush likely occurred at ~800° to 720 °C at a depth of no <15–12 km as the H_2O content increased from ~4–5% to ~7.5%.

8. Eruption environment

Silicic magmas containing Mn-rich garnets are commonly associated with extensional conditions (Harangi et al., 2001), as is the case for the

Ramada Volcanic Center, which was emplaced on the eastern margin of the NW-SE trending Olacapato-El Toro fault zone as extensional faulting and mafic volcanism appeared to the south (e.g., Risse et al., 2008). Regional and local structural and magmatic studies have long highlighted the transtensional and extensional movements on the Olacapato-El Toro fault system relative to the Miocene eruptions of the Negra Muerta and Aguas Calientes calderas and the Quaternary monogenetic basaltic and shoshonitic cones (e.g., San Geronimo and Negro de Chorrillos) and Tocomar rhyolite (Petrinovic et al., 2006; Riller et al., 2001; Viramonte et al., 1984). In this context, the trans-tensional Olacapato-El Toro shear zone represents a long-lasting inherent weakness along which strike-slip and normal Neogene faults are localized in a structural transfer zone that accommodates the motion of orogen-parallel thrust faults to the north and south (e.g., Acocella et al., 2011; Norini et al., 2013).

From a volcanic perspective, the ~6.3 k ± 0.3 Ma Ramadas Volcanic Center is essentially unique in being the largest late Neogene plinian rhyolitic eruption in the Puna with Tait (2004) calculating an ejected volume of ~36 km^3 DRE and a column height of ~39 km above the vent. This plinian eruption style contrasts sharply with that of the giant dacitic ignimbrites without significant fall deposits that erupted in the Puna-Altiplano ignimbrite flare-up over the <10 Ma (e.g., de Silva and Francis, 1991; Coira et al., 1993; Kay and Coira, 2009; Kay et al., 2010). Their relative lack of fall deposits has been attributed to wide radius source vents that in the relatively low density atmosphere above 3800 m a.s.l. in the Altiplano–Puna leads to a negative buoyancy that induces column collapse in response to reductions of the velocity in the gas thrust region and the rate of air entrainment in the convective region (Bursik and Woods, 1991). In contrast, Tait (2004) argues that the Ramadas Volcanic Center plinian eruption was ejected from a flaring point source vent that led to a buoyant column and a crystal-poor, high velocity eruption. The preservation of the spessartine-rich garnet in the tuff suggests this flaring point was only somewhat shallower than the ~12–15 km depth at which the garnet crystallized from the extracted rhyolite magma.

9. Final discussion and conclusions

Spessartine-rich garnet phenocryst with distinctive compositions ($Alm_{70-72}Sps_{22-25}Grs_{3-4}Prp_{05-1}$) in peraluminous rhyolite tephra layers in the Neogene Guanaco Formation of the foreland basin deposits in Argentina east of the Puna plateau serve both as markers for correlating foreland strata and in identifying their eruptive source as the Ramadas Volcanic Center on the eastern margin of the Puna along the Olacapato-El Toro lineament, ~120 to 200 km to the north and west.

New Ar/Ar age determinations for the Guanaco tuffs in conjunction with previous dating of the Corte Blanco tuffs show that the Ramadas Volcanic Center eruptions occurred between 5.9 and 6.4 Ma and most probably close to 6.3 Ma.

Like the less spessartine-rich garnet-bearing Coyaguayma Ignimbrite (Caffe et al., 2012) to the north, the Ramadas tuffs are best interpreted as mafic magmas contaminated by assimilation and dehydration melts of Neoproterozoic-Eocambrian Puncoviscana Fm. Mn-bearing metasediments and average Puna basement. Supporting evidence comes from their newly recalculated $^{87}Sr/^{86}Sr$ initial ratios (~0.71192) and $^{143}Nd/^{144}Nd$ initial ratios (0.52337, εNd ~−7) along with pronounced Pb spikes on trace element diagrams. On a regional scale, the Ramadas tuffs are slightly more isotopically enriched than the ~6 to 2 Ma Galan Ignimbrites to the south and the nearby ~10 Ma Aguas Calientes tuffs, and less radiogenic than the ~11 Ma garnet-bearing Coyaguayma ignimbrites. Like the Cerro Galan ignimbrites, the isotopic characteristics of the Ramadas tuffs are consistent with their being ~50–50 mixtures of mantle-derived mafic and crustal-derived melts.

The major and trace element chemistry of the Ramadas Volcanic Center spessartine-rich garnet-bearing rhyolitic magmas is best interpreted as reflecting eruption of a late stage melt segregation from a mid-crustal crystalline mush that left behind plagioclase, potassium feldspar, biotite and quartz crystals along with accessory zircon, apatite and allanite. Essentially the only mineral to crystallize from the separated rhyolite before the plinian eruption was spessartine-rich garnet that is found as euhedral phenocrysts among the pumice fragments. Feldspar fractionation is supported by extreme negative Eu anomalies and very low Sr and Ba concentrations and zircon, apatite and allanite loss by the shape of the REE patterns and low Zr concentrations.

Unlike the more crystal-rich spessartine-rich garnet-bearing Coyaguayma tuffs, the only major mineral in the segregated melt before the explosive eruption of the Ramadas ignimbrite was a small amount of Mn-rich garnet signaling a pre-eruption crystallization at depths of ~15–12 km. The presence of both blocky and bubble wall shards in the distal ash deposits of the Guanaco Formation Tuffs is consistent with an initial vent-opening associated with a series of pulsating phreatic magmatic surges, which were almost immediately entrained into the Plinian eruption of the garnet-bearing Ramadas Volcanic Center rhyolites.

The eruption was likely triggered by transtension along the Olacapato-El Toro lineament (Norini et al., 2013) and could have been facilitated by underplating of a mafic shoshonitic series magma, whose presence is signaled by relict resorbed Mg-rich hornblende and biotite xenocrysts in the Ramadas tuffs. The eruption could have been associated with foundering of the underlying lithospheric removal as suggested by Kay et al. (1994) and Kay et al. (2010).

Acknowledgements

This research was funded by the Agencia Nacional de Promoción Científica y Tecnológica PICT-2012-1984 and PICT-2014-3436, and Universidad Nacional de Jujuy (Secretaría de Ciencia y Técnica y Estudios Regionales 08/E036 and 08/E037), Argentina and the Snee Professorship at Cornell University. We thank Patrocinio Flores, Roberto Liquin and Paulino Cachizumba for their support in laboratory work in Jujuy and Silvia Rosas for her assistance with graphics. Thanks are also due to C. H. Chung of the Geochronology Laboratory, National Taiwan University for the Ar/Ar ages of some of the glasses. The paper was improved by the perceptive comments of reviewer Eugenio Aragón.

Appendix A. Analytical methods

Whole rock analyses of the tuffs were done on rock powders. Major elements, Y, Rb, Pb, Zr and Nb were analyzed on a Rigaku FX2000 instrument at the University of Jujuy, Argentina using the methods described in Caffe et al. (2002). Analyses for Fe, Na, La, Ce, Nd, Sm, Eu, Tb, Yb, Lu, Sr, Ba, Cs, U, Th, Hf, Ta, Sc, Cr, Ni and Co were done by Instrumental Neutron Activation Analyses (INAA) at Cornell University as described by Kay et al. (1999) and Kay et al. (2010). The Fe content of each sample was used as an internal flux monitor in the INAA analyses. The absolute element concentrations reported in the INAA analyses are based on Fe concentrations calculated using the sample weight and the live counting time at a constant distance from the detector. Where Ba analyses differed, INAA analyses are reported. INAA precision and accuracy based on replicate analyses of internal standards are 2–5% (2 sigma) for most elements and 10% for Sr, Nd and Ni at low concentrations. Supplementary data to this article can be found online at https://doi.org/10.1016/j.jvolgeores.2018.08.020.

References

Acocella, V., Gioncada, A., Omarini, R., Riller, U., Mazzuoli, R., Vezzoli, L., 2011. Tectonomagmatic characteristics of the back-arc portion of the Calama–Olacapato–El Toro Fault Zone, Central Andes. Tectonics 30, TC3005.

Arias, J.E., Alonso, R., Malanca, S., 1978. Un gliptodontoideo de la Formación Piquete (Grupo Orán) Provincia de Jujuy, República Argentina. Rev. Inst. Cienc. Geol. 3, 175–188.

Bardelli, L., Viramonte, J.G., Giordano, G., De Astis, G., Becchio, R., Lucci, F., Baez, W., 2017. Granates de unidad rio líticas del centro volcánico Mioceno Ramada, Andes Centrales, Provincia de Salta (NO Argentina): Posible temperatura de cristalización y discusiones petrogenéticas. XX Congreso Argentino, San Miguel de Tucumán, 7–11 de augusto, sesión A4. pp. 7–14.

Bigazzi, G., 2004. Fission track dating of the Corte Blanco Tuff. In: Tait, M.A. (Ed.), Dynamics Eruption Dynamics and Evolution of a Highly Explosive Rhyolitic Volcanic Complex in the High Andes: The Late Miocene Ramadas Volcanic Centre, Andean Puna, Salta Argentina. Monash University, Melbourne, Australia (Ph.D. Thesis).

Bursik, M., Woods, A., 1991. Buoyant, super-buoyant and collapsing eruption columns. J. Volcanol. Geotherm. Res. 45, 347–350.

Caffe, P.J., Trumbull, R.B., Coira, B.L., Romer, R.L., 2002. Petrogenesis of early Neogene magmatism in the northern Puna; implications for magma genesis and crustal processes in the Central Andean plateau. J. Petrol. 43, 907–942.

Caffe, P.J., Trumbull, R.B., Siebel, W., 2012. Petrology of the Coyaguayma ignimbrite, northern Puna of Argentina: Origin and evolution of a peraluminous high-SiO_2 rhyolite magma. Lithos 134–135, 179–200.

Chesner, C.A., Rose, W.I., Deino, A., Drake, R., Westgate, J.A., 1991. Eruptive history of Earth's largest Quaternary caldera (Toba, Indonesia) clarified. Geology 19, 200–203.

Coira, B., Kay, S.M., Viramonte, J., 1993. Upper Cenozoic magmatism of the Argentina Puna. Int. Geol. Rev. 35, 677–720.

Dahlquist, J.A., Galindo, C., Pankhurst, R.J., Rapela, C.W., Alasino, P.H., Saavedra, J., Fanning, C.M., 2007. Magmatic evolution of the Peñón Rosado granite: petrogenesis of garnet-bearing granitoids. Lithos 95, 177–207.

Del Papa, C.E., Disalvo, A., Reynolds, J., Pereyra, R., Viramonte, J.G., 1993. Utilización de niveles piroclásticos en correlaciones estratigráficas: Un ejemplo para el Terciario Superior del noroeste argentino. 12° Congreso Geológico Argentino y 2° Congreso de Exploración de Hidrocarburos, Actas. vol. 2. Asociación Geológica Argentina, Mendoza, pp. 166–171.

Déruelle, B., 1991. Petrology of Quaternary shoshonitic lavas of northwestern Argentina. Geol. Soc. Am. Spec. Pap. 265, 201–216.

Francis, P.W., Sparks, R.S.J., Hawkesworth, C.J., Thorpe, R.S., Pyle, D.M., Tait, S.R., Mantovani, M.S., McDermott, R., 1989. Petrology and geochemistry of volcanic rocks of the Cerro Galán caldera, northwest Argentina. Geol. Mag. 126, 515–547.

Frost, C.D., Frost, B.R., Beard, J.S., 2016. Review: on silica-rich granitoids and their eruptive equivalents. Am. Mineral. 101, 1268–1284.

Galli, C.E., 1995. Estratigrafía y sedimentología del Subgroupo Metan (Grupo Oran, Terciario), provincia de Salta, Argentina. (Ph.D. Thesis). Universidad Nacional de Salta, Salta, Argentina (109 pp.).

Gauthier, P.J., Déruelle, B., Viramonte, J., Aparicio, A., 1994. Grenats des rhyolites de la caldera de La Pava-Ramada (NW Argentine) at de leursxénolites granitiques. Comptes Rendeus Acad. Sci. Paris 318 (serie II), 1629–1635.

Gebhard, J., Giudici, A.R., Oliver Gascon, J., 1974. Geología de la comarca entre el río Juramento y arroyo Las Tortugas, provincias de Salta y Jujuy, República Argentina. Rev. Asoc. Geol. Argent. 29, 359–375.

González Villa, R.E., 2002. El Subgrupo Jujuy (Neógeno) entre los 24°–26° LS y 64°–66° LO, tramo centro-austral de la cadena Subandina argentina, provincias de Salta y Jujuy. (PhD thesis). Facultad de Ciencias Naturales, Universidad Nacional de Salta, Argentina (291 pp.).

Green, T.H., 1977. Garnet in silicic liquids and its possible use as a P–T indicator. Contrib. Mineral. Petrol. 65, 59–67.

Green, T.H., 1992. Experimental phase equilibrium studies of garnet bearing I-type volcanics and high-level intrusives from Northland, New Zealand. Trans. R. Soc. Edinb. Earth Sci. 83, 429–438.

Harangi, S., Downes, H., Kosa, L., Szabo, C., Thirlwall, M.F., Mason, P.R.D., Mattey, D., 2001. Almandine garnet in calc-alkaline volcanic rocks of the Northern Pannonian Basin (Eastern-Central Europe): geochemistry, petrogenesis and geodynamic implications. J. Petrol. 42, 1813–1843.

Kay, S.M., Coira, B.L., 2009. Shallowing and steepening subduction zones, continental lithospheric loss, magmatism, and crustal flow under the Central Andean Altiplano–Puna Plateau. In: Kay, S.M., Ramos, V.A., Dickinson, W.R. (Eds.), Backbone of the Americas: Plateau Uplift, Shallow Subduction and Ridge Collision. Geological Society of America Memoir vol. 204. Geological Society of America, Boulder CO, pp. 229–259.

Kay, S.M., Coira, B., Viramonte, J., 1994. Young mafic back-arc volcanic rocks as indicators of continental lithospheric delamination beneath the Argentine Puna plateau, Central Andes. J. Geophys. Res. 99, 24323–24339.

Kay, S.M., Mpodozis, C., Coira, B., 1999. Magmatism, tectonism and mineral deposits of the Central Andes (22°–33°S latitude). In: Skinner, B.J. (Ed.), Geology and Ore Deposits of the Central Andes: Society of Economic Geology Special Publication 7, pp. 27–59.

Kay, S.M., Coira, B.L., Caffe, P.J., Chen, C.-H., 2010. Regional chemical diversity, crustal and mantle sources and evolution of the Neogene Puna plateau ignimbrites of the Central Andes. J. Volcanol. Geotherm. Res. 198, 81–111.

Kay, S.M., Coira, B., Woerner, G., Kay, R.W., Singer, B.S., 2011. Geochemical, isotopic and single crystal $^{40}Ar/^{39}Ar$ age constraints on the evolution of the Cerro Galan ignimbrites. Bull. Volcanol. 73, 1487–1511.

Layer, P.W., Hall, C.M., York, D., 1987. The derivation of $^{40}Ar/^{39}Ar$ age spectra of single grains of hornblende and biotite by laser step heating. Geophys. Res. Lett. 14, 757–760.

Leake, B.E., Woolley, A.R., Arps, C.E.S., Birch, W.D., Gilbert, M.C., Grice, J.D., Hawthorne, F.C., Kato, A., Kisch, H.J., Krivovichev, V.G., Linthout, K., Laird, J., Mandarino, J., Maresch, W.V., Nickel, E.H., Schumaker, J.C., Smith, D.C., Stephenson, N.C.N., Ungaretti, L., Whittaker, E.J.W., Youzhi, G., 1997. Nomenclature of amphiboles: report of the subcommittee on amphiboles of the International Mineralogical Association Commission on New Minerals and Mineral Names. Am. Mineral. 82, 1019–1037.

Lo, C.-H., Chung, S.-L., Lee, T.-Y., Wu, G.-Y., 2002. Age of the Emeishan flood magmatism and relations to Permian-Triassic boundary events. Earth Planet. Sci. Lett. 198, 449–458.

Lucassen, F., Becchio, R., Harmon, R., Kasemann, S., Franz, G., Trumbull, R., Wilke, H.-G., Romer, R.L., Dulski, P., 2001. Composition and density model of the continental crust at an active continental margin — the central Andes between 21° and 27° S. Tectonophysics 341, 195–223.

Maro, G., Caffe, P., Romer, R.L., Trumbull, R.B., 2017. Neogene Mafic Magmatism in the Northern Puna Plateau, Argentina: Generation and Evolution of a Back-arc Volcanic Suite. vol. 58 pp. 1591–1618.

Matteini, M., Mazzuoli, R., Omarini, R., Cas, R., Maas, R., 2002a. The geochemical variations of the upper Cenozoic volcanism along the Calama–Olocapato–El Toro transversal fault system in central Andes (24°S): petrogenetic and geodynamic implications. Tectonophysics 345, 211–227.

Matteini, M., Mazzuoli, R., Omarini, R., Cas, R., Maas, R., 2002b. Geodynamical evolution of the central Andes at 24°S as inferred by magma composition along the Calama–Olocapato–El Toro transversal volcanic belt. J. Volcanol. Geotherm. Res. 118, 205–228.

Mazzuoli, R., Vezzoli, L., Omarini, R., Acocella, V., Gioncada, A., Matteini, M., Dini, A., Guillou, H., Hauser, N., Uttini, A., Scaillet, S., 2008. Miocene magmatism and tectonics in the easternmost sector of the Calama–Olocapato–El Toro fault system in Central Andes at 24°S: insights into the Eastern Cordillera evolution. Geol. Soc. Am. Bull. 120, 1493–1517.

McPhie, J., Doyle, M., Allen, R., 1993. Volcanic Textures. A Guide to the Interpretation of Textures in Volcanic Rocks. Centre for Ore Deposit and Exploration Studies, Tasmania (198 pp.).

Miller, C.F., Stoddard, E.F., 1981. The role of manganese in the paragenesis of magmatic garnet: an example from the Old Woman Piute Range, California. J. Geol. 89, 233–246.

Norini, G., Baez, W., Becchio, R., Viramonte, J., Giordano, G., Arnosio, M., Pinton, A., Groppelli, G., 2013. The Calama–Olacapato–El Toro fault system in the Puna Plateau, Central Andes: geodynamic implications and stratovolcanoes emplacement. Tectonophysics 608, 1280–1297.

Petrinovic, I.A., Mitjavilla, J., Viramonte, J.G., Marti, J., Becchio, R., Arnosio, M., Colombo, F., 1999. Geoquímica y geocronología de las secuencias neógenas de trasarco, en el extremo oriental de la cadena volcánica transversal del Quevar, noroeste de Argentina. Acta Geol. Hisp. 34, 255–273.

Petrinovic, I.A., Riller, U., Brod, J.A., Alvarado, G., Arnosio, M., 2006. Bimodal volcanism in a tectonic transfer zone: evidence for tectonically controlled magmatism in the southern Central Andes, NW Argentina. J. Volcanol. Geotherm. Res. 152, 240–252.

Richards, J.P., Ulrich, T., Kerrick, R., 2006. The late Miocene Quaternary Antofalla volcanic complex, southern Puna, NW Argentina: protracted history, diverse petrology and economic potential. J. Volcanol. Geotherm. Res. 152, 197–239.

Ridolfi, F., Rensulli, A., Puerini, M., 2010. Stability and chemical equilibrium of amphibole in calc-alkaline magmas: an overview, new thermobarometric formulations and application to subduction-related volcanoes. Contrib. Mineral. Petrol. 16, 45–66.

Riller, U., Petrinovic, I., Ramelow, J., Strecker, M., Oncken, O., 2001. Late Cenozoic tectonism, collapse caldera and plateau formation in the central Andes. Earth Planet. Sci. Lett. 188, 299–311.

Risse, A., Trumbull, R.B., Coira, B., Kay, S.M., van den Bogaard, P., 2008. $^{40}Ar/^{39}Ar$ geochronology of basaltic volcanism in the back-arc region of the southern Puna plateau Argentina. J. S. Am. Earth Sci. 26, 1–15.

Russo, A., Serraiotto, A., 1978. Contribución al conocimiento de la estratigrafía terciaria en el noroeste Argentino. VII Congreso Geológico Argentino Actas I, pp. 715–730.

Salfity, J.A., Marquillas, R.A., 1994. Tectonic and sedimentary evolution of the Cretaceous-Eocene Salta Group Basin, Argentina. In: Salfity, J.A. (Ed.), Cretaceous Tectonics of the Andes. Earth Evolution Sciences. Fried. Vieweg and Sohn, Germany, pp. 266–315.

Schmidt, G.I., Montalvo, C.I., Sostillo, R., Cerdeno, 2018. Proterotheriidae (Mammalia, Litopterna) from the Cerro Azul Formation (late Miocene), La Pampa Province, Argentina. J. S. Am. Earth Sci. 83, 165–177.

de Silva, S.L., Francis, R.W., 1991. Volcanoes of the Central Andes. Springer-Verlag, New York (216 pp.).

Sparks, R.S.J., Walker, G.P.L., 1977. The significance of vitric-enriched air-fall ashes associated with crystal-enriched ignimbrites. J. Volcanol. Geotherm. Res. 2, 329–341.

Sun, S.-s., McDonough, W.F., 1989. Chemical and isotopic systematics of oceanic basalts; implications for mantle composition and processes. In: Saunders, A.D., Norry, M.J. (Eds.), Magmatism in the Ocean Basins. Geol. Soc. Special Publication 42, pp. 313–42,345.

Tait, M.A., 2004. Dynamics of a Large Volume Plinian Eruption: Dispersal of the Late Miocene Corte Blanco Tuff, Ramadas Volcanic Centre, Andes Mountains, Salta, Argentina. (Ph.D. Thesis). Monash University, Melbourne, Australia, p. 254.

Tait, M.A., Cas, R.A.F., Viramonte, J.G., 2009. The origin of an unusual tuff ring of perlitic rhyolite pyroclasts: the last explosive phase of the Ramada Volcanic Centre, Andean Puna, Salta, NW Argentina. J. Volcanol. Geotherm. Res. 183, 1–16.

Viramonte, J.G., Omarini, R.H., Araña Saavedra, V., Aparicio, A., García Cacho, I., Parica, R., 1984. Edad, génesis y mecanismos de erupción de las riolitas granatíferas de San Antonio de los Cobres, provincia de Salta. IX Congreso Geológico Argentino Actas. vol. 3, pp. 216–233.

Viramonte, J.G., Reynolds, J.H., del Papa, C., Disalvo, A., 1994. The Corte Blanco garnetiferous tuff: a distinctive Late Miocene marker bed in Northwestern Argentina applied to magnetic polarity stratigraphy in the Rio Yacones, Salta Province. Earth Planet. Sci. Lett. 121, 519–531.

Viramonte, J.M., Viramonte, J.G., Becchio, R., Pimentel, M., Arnosio, M., 2007. Ramada volcanic center (NW-Argentina): linking between the Miocene volcanism and the lower Paleozoic basement. 20th Colloquium on Latin American Earth Sciences. Abstracts, pp. 62–63 (Kiel, Germany).

Winchester, J.A., Floyd, P.A., 1977. Geochemical discrimination of different magma series and their differentiation products using immobile elements. Chem. Geol. 20, 325–343.

Wohletz, K.H., 1983. Mechanisms of hydrovolcanic pyroclastic formation: grain-size, scanning electron microscopy, and experimental studies. J. Volcanol. Geotherm. Res. 17, 31–63.